NASA Contractor Report 3674

Test Results of Modified Electrical Charged Particle Generator for Application to Fog Dispersal

Walter Frost and Kao-Huah Huang

CONTRACT NAS8-34729
FEBRUARY 1983

NASA

NASA Contractor Report 3674

Test Results of Modified Electrical Charged Particle Generator for Application to Fog Dispersal

Walter Frost and Kao-Huah Huang
FWG Associates, Inc.
Tullahoma, Tennessee

Prepared for
George C. Marshall Space Flight Center
under Contract NAS8-34729

National Aeronautics
and Space Administration

Scientific and Technical
Information Branch

1983

ACKNOWLEDGMENTS

The work reported herein was supported by the National Aeronautics and Space Administration, Marshall Space Flight Center, Space Science Laboratory, Atmospheric Sciences Division, under Contract NAS8-34729.

The authors are indebted to Mr. A. Richard Tobiason of the Office of Aeronautics and Space Technology (OAST), NASA Headquarters, Washington, D.C., for his support of this research. Special thanks are given to Mr. Dennis W. Camp (scientific monitor of the program) and Dr. Bob Smith of Marshall Space Flight Center who provided considerable technical advice and input to the final documentation. Also, the authors are appreciative of the technical discussions with Dr. Lothar Ruhnke of the Naval Research Laboratory, Washington, D.C.

TABLE OF CONTENTS

LIST OF ILLUSTRATIONS

LIST OF SYMBOLS

Symbol	Definition
A	Cross section area of particle
C/M	Charge mass ratio
C_D	Drag coefficient
d	Particle diameter
d_o	Nozzle diameter at exit
E(0)	Electrical field strength at the exit of nozzle
E(r)	Radial electrical field strength function
E(z)	Vertical electrical field strength function
$E_m(z)$	Maximum radial electrical field strength at height z
E_{rmax}	Maximum radial electrical field strength
$E_{x,y,z}$	Three components of electrical field strength
$F_{ex,ey,ez}$	Three components of electrical force
g	Acceleration of gravity
H	Vertical distance from nozzle exit to needle probe
HVP	High-voltage probe
I	Current
L	Nozzle length
m	Mass of particle
n	Number of charges on each particle
P_1	Stagnation pressure
q_p	Charges on the droplet
q_{ps}	Saturation charge on the particle

Symbol	Definition
R	Radius where the radial electrical field strength is a maximum
RH	Relative humidity
R_j	Radius of the exit nozzle
r	Radial distance from the center of the jet
t	Time
U_m	Axial velocity at center of the jet
U_o	Velocity at the exit of the nozzle
u	Axial velocity of the jet
V	Average airflow velocity in the nozzle
$\|V_a\|$	Magnitude of the particle velocity relative to the air
v	Radial velocity of the jet
$W_{x,y,z}$	Three instantaneous wind velocity components
x,y,z	Cartesian coordinates with the origin at the center of the nozzle exit and z direction upward
z	Height measured from the exit of nozzle
z_m	Height above nozzle exit plane where voltage is maximum

Greek Symbols

α	Ratio of jet velocity at the exit of nozzle to the velocity of crosswind U_o/U_1
ϵ_o	Permitivity of free space
η	Curved distance along the jet centerline
ξ	Ratio of radial distance to vertical distance ($\xi = \sigma r/z$, $\sigma = 18.5$)
ρ_a	Air density
ρ_e	Charge density

1.0 INTRODUCTION

Under NASA Contract NAS8-33541, a prototype of a fog dispersal unit was built and preliminary performance tests carried out. A general description of the system and discussion of the results are presented in the final report from that contract (Frost 1982). A major conclusion by Frost (1982) was that a number of significant design modifications need to be investigated. These modifications have been made and follow-on testing has been carried out. Beneficial experience toward the design of both a second-generation operational-type unit and of an advanced research-type unit has been obtained from these tests. The major modifications were made to the nozzle and to the flow control system. Moreover, a new system of instrumentation to record the current output and to measure the voltage drop at the corona was developed.

This report describes the modifications to and subsequent testing of the charged particle generator. Section 2.0 describes the hardware modifications to the experimental apparatus. Section 3.0 presents the results and compares these with previous results reported by Frost (1982). The results are interpreted in terms of improvements to the performance of the system. Section 4.0 presents the conclusions relative to the modified prototype unit.

2.0 EXPERIMENTAL APPARATUS

Modifications to the previous fog dispersal unit under this contract effort are reported in this section. Each modification is described and compared with the previous system arrangement. The description of the experimental apparatus was divided into five sections in the last report. These sections were: (1) air supply circuit, (2) nozzle, (3) water flow circuit, (4) electrical circuit, and (5) current output measurement circuit. The modification to each of these categories is described in the following subsections.

2.1 Air Supply Circuit

The general arrangement of the experimental apparatus is illustrated in Figure 2.1. The previous arrangement used the compressor to supply the airflow through the nozzle and to act as a high-pressure source to drive the water flow. However, this arrangement resulted in poor control of the water flow rate. Consequently, a separate positive displacement pump was added to the system to pump the water, and the compressor was used only to supply airflow through the nozzle. Other than this modification, the air supply circuit remains the same.

2.2 Nozzle

A new converging/diverging nozzle was cast out of Plexiglas. This nozzle was cast with an attractor at the throat and was designed for an exit Mach number of 1.35. The nozzle used on the original prototype system was also designed for a Mach number of 1.35; however, due to the necessity of using a thicker corona needle than originally planned, the nozzle did not perform as designed. The geometry of the new nozzle was designed to account for this blockage effect. In actual fact, the geometry of the new nozzle is not different in dimensions from that of

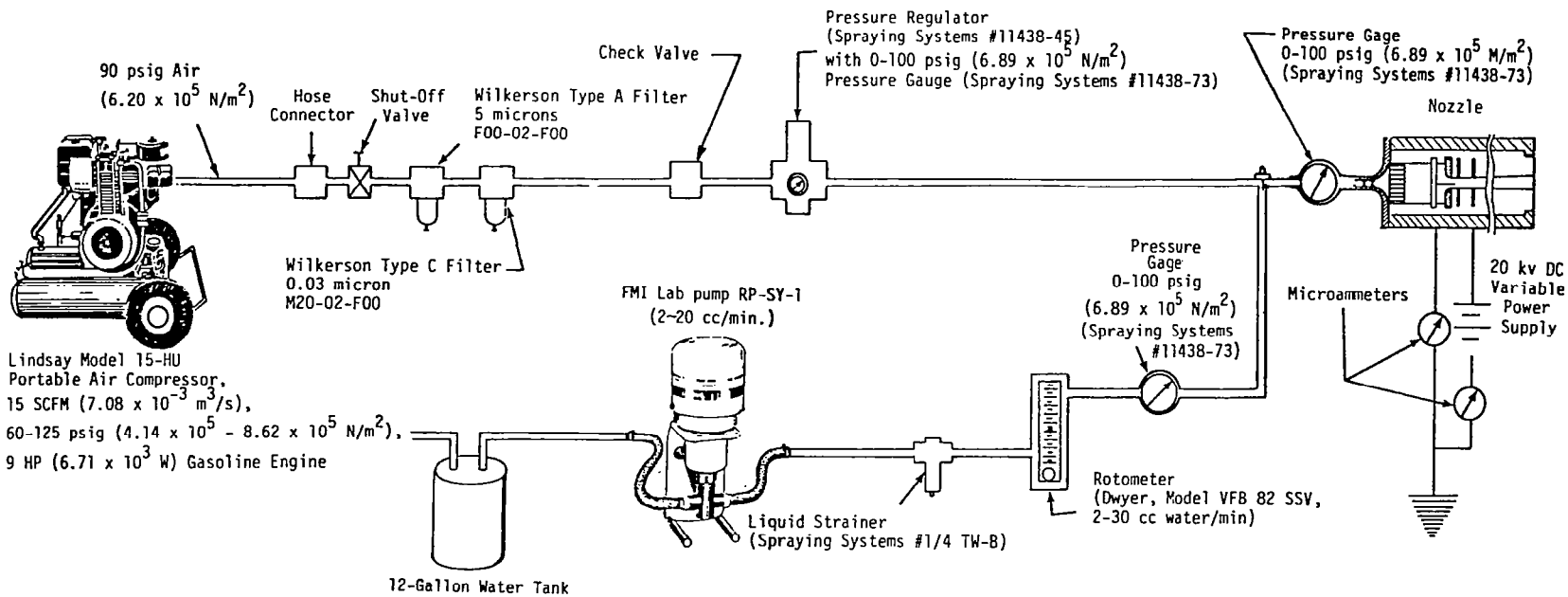

NOTE: All plumbing is 1/4" (0.64 cm) galvanized steel pipe.

Figure 2.1 Schematic of charged particle generator.

the previous nozzle because the attractor is now at the throat and the needle does not protrude into the throat region, and hence does not reduce the actual throat area.

The cross sectional area of the throat controls the Mach number at the exit for a given pressure difference across the nozzle. Again, however, difficulties were encountered with this new nozzle. During casting of the nozzle, a good seal between the wire running to the attractor and the Plexiglas was not achieved. Consequently, water and air leaked through this region. Arcing thus occurred at high-voltage settings and eventually burned out the wire. Consequently, the nozzle was not useful for further testing, and all results reported herein are for tests utilizing the older nozzle.

2.3 Water Flow Circuit

Liquid water is supplied from a 12-gallon tank. The tank was originally pressurized with bleed airflow from the primary airflow used to supply the nozzle. With this arrangement, extreme difficulty in controlling the liquid water flow rate was encountered. Therefore, a FMI* laboratory pump RP-SY-1 was installed in the water supply circuit and the pressure bleed airflow arrangement disconnected. The water is now pumped from the water tank through a rotameter to the atomizer valve. Figure 2.2 is a photograph of the water pump. The RP-SY-1 laboratory pump can control the flow rate from 1.9 cc/min to 19.4 cc/min and can attain head pressure up to 60 psi.

2.4 Electrical Circuit

A 20,000 volt power supply with a variable rheostat control circuit, as described in Frost (1982), was used for all tests carried out in this study. The voltage drop across the attractor and needle was measured

---

*Trade name of FMI Fluid Metering, Inc., 29 Orchard Street, Oyster Bay, NY 11771.

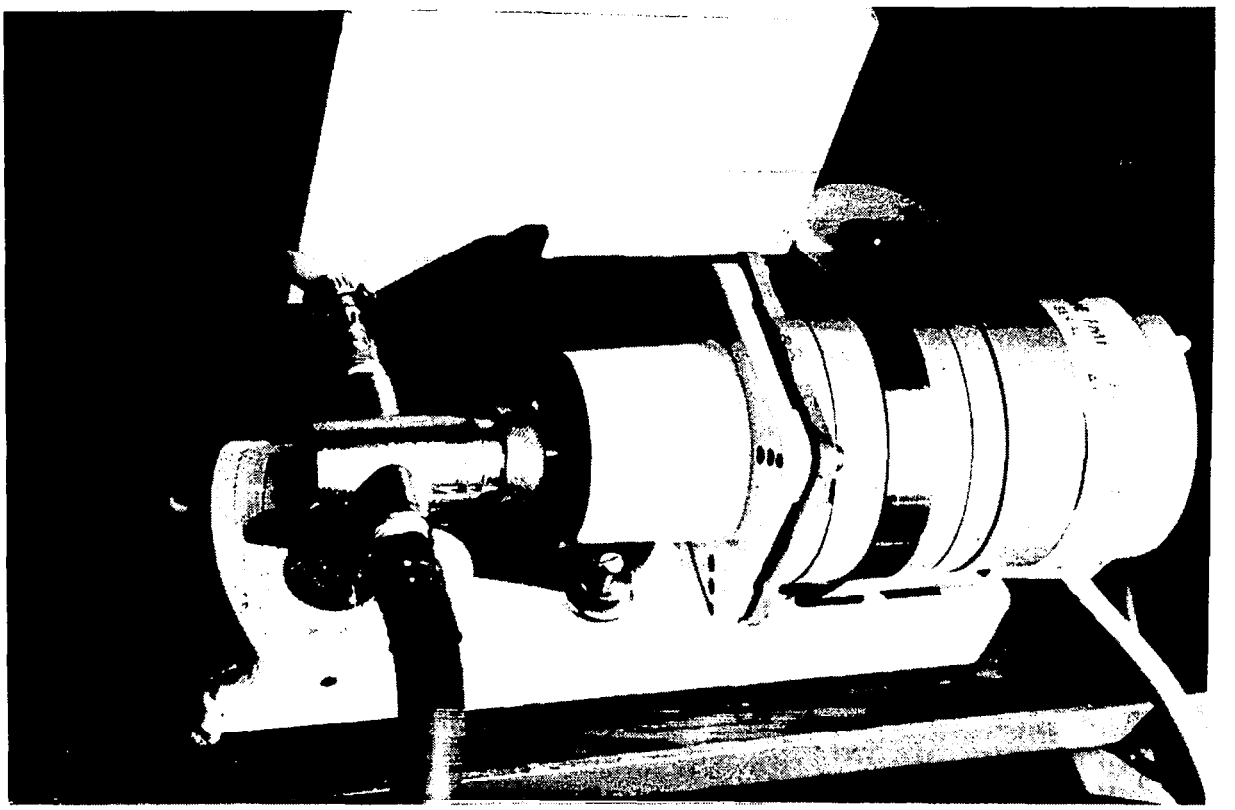

Figure 2.2 FMI RP-SY-1 water pump.

with a B&K** 3-1/2-digit digital multimeter connected with a B&K PR-28 high-voltage probe (see Appendix A). The probe was placed in the circuit, as shown in Figure 2.3. Using the PR-28 high-voltage probe coupled with the digital multi-range voltmeter, voltages up to 40 kV DC can be measured to ±3 percent accuracy. The high-voltage probe proved very successful in measuring both the voltage drop across the corona and the voltage along the centerline of the jet.

2.5 Current Output Measurement Circuit

Two output current measuring systems were used for the present tests. One was the previously used grounded needle arrangement

---

**Trade name of Dynascan Corporation, 6460 West Cortland Street, Chicago, IL 60635.

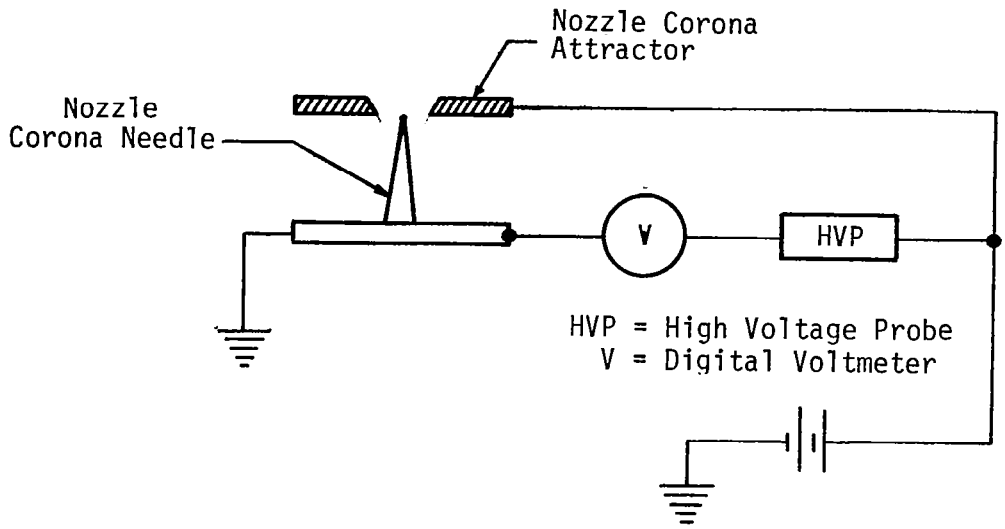

Figure 2.3 Circuit for measuring the voltage drop across the gap between the corona attractor and needle.

(Frost 1982). The other was a current collection system, based on discussions with Lothar Ruhnke of the Naval Research Laboratory. This system consisted of a conductive cylinder placed over the jet to collect all charges exiting the nozzle. The cylinder was grounded through an ammeter, which measured the current in the jet. This cylinder was 6 inches in diameter, 2 feet long, and covered on the top with an aluminum mesh. The configuration of this collection system is shown in Figure 2.4. The following reported measurements of output current have been made with both the new collection system (labeled pipe measurement) and the previously used needle probe system (labeled needle measurement).

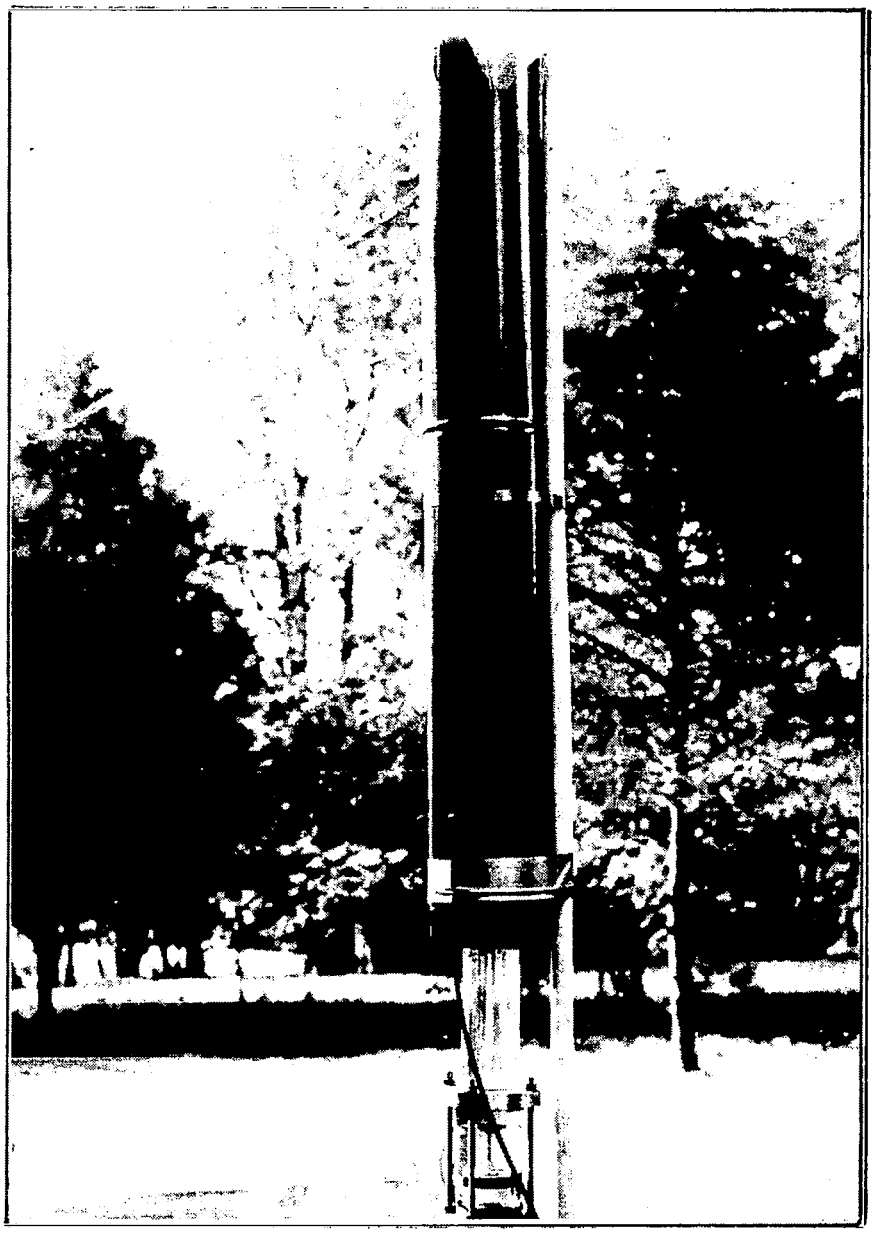

Figure 2.4 Charged droplet collection pipe.

3.0 RESULTS AND DISCUSSION

Results of the tests carried out are discussed in this section. The output current with variation of the controllable parameters is the primary variable measured. Comparison with previous results is also given and the effects of modification to the previous system described. In addition, measured velocity and voltage distributions along the jet not made during the previous study are discussed.

3.1 Current Output

As in the previous report (Frost 1982), the controllable parameters include: (1) the liquid water flow rate, (2) the corona voltage, and (3) the nozzle stagnation pressure. Figure 3.1 schematically illustrates the measurement arrangement. The current output measurements include both those made with the pipe system and those made with the needle probe. Comparison is made with previous results.

3.1.1 Liquid Water Flow Rate

The variation of the electrical current of the jet with liquid water flow rate is shown in Figure 3.2. In this figure, the current output is scaled by the stagnation pressure and the relative humidity, RH, of the atmosphere. The output current was found to scale with RH empirically. This effect is believed to be associated with the dependence of the electrical conductivity of the atmospheric air on RH. Conductivity will increase with increasing RH allowing more current to leak to ground in preference to flowing through the measuring probe. Thus, under very dry conditions, a higher jet current measurement is anticipated.

Results for both the needle measurement and the pipe measurement are shown on the figure for the same test. These measurements were made by changing probes without shutting down the system or changing the

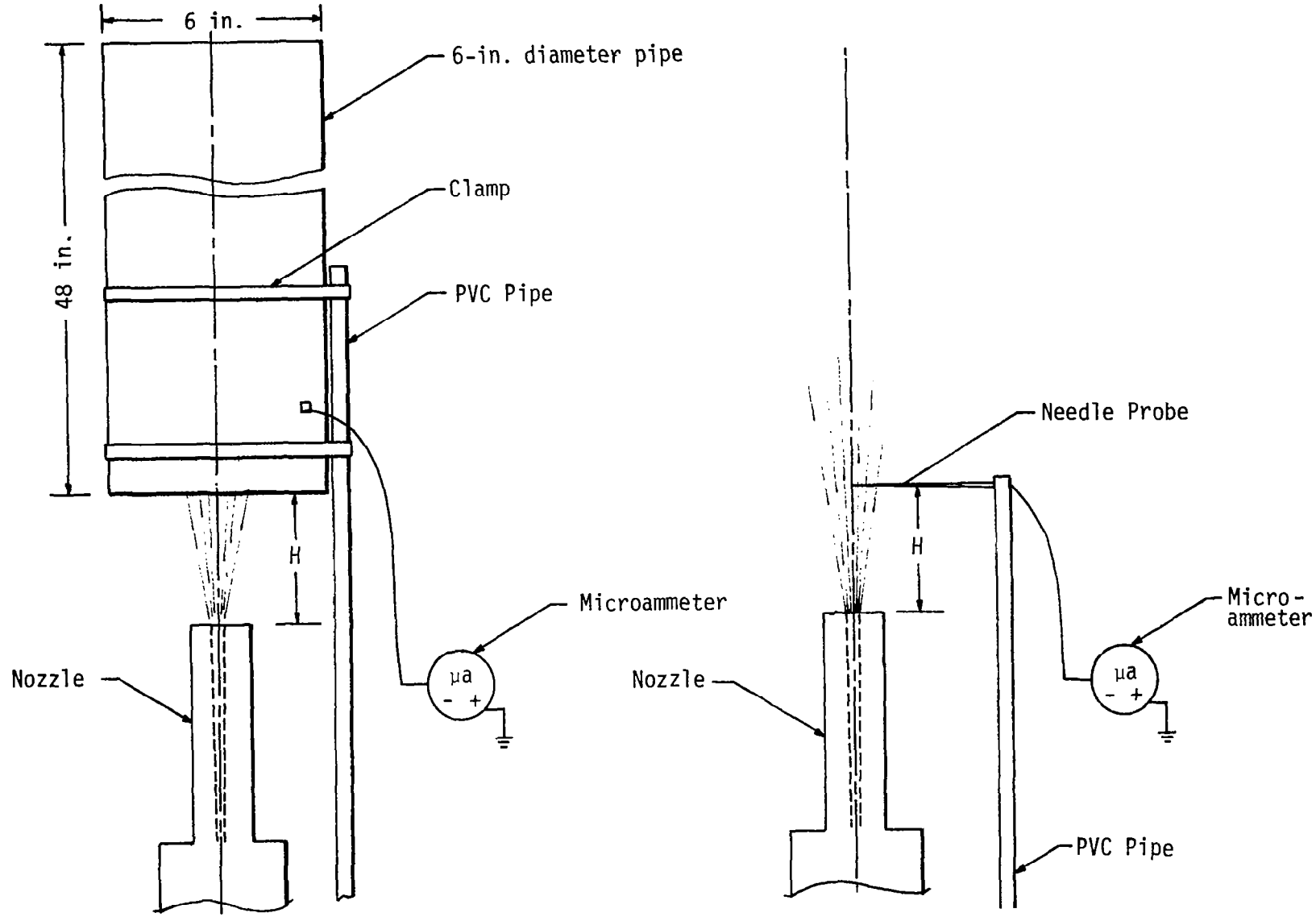

Figure 3.1 Schematic of output current measurement with pipe and needle probe.

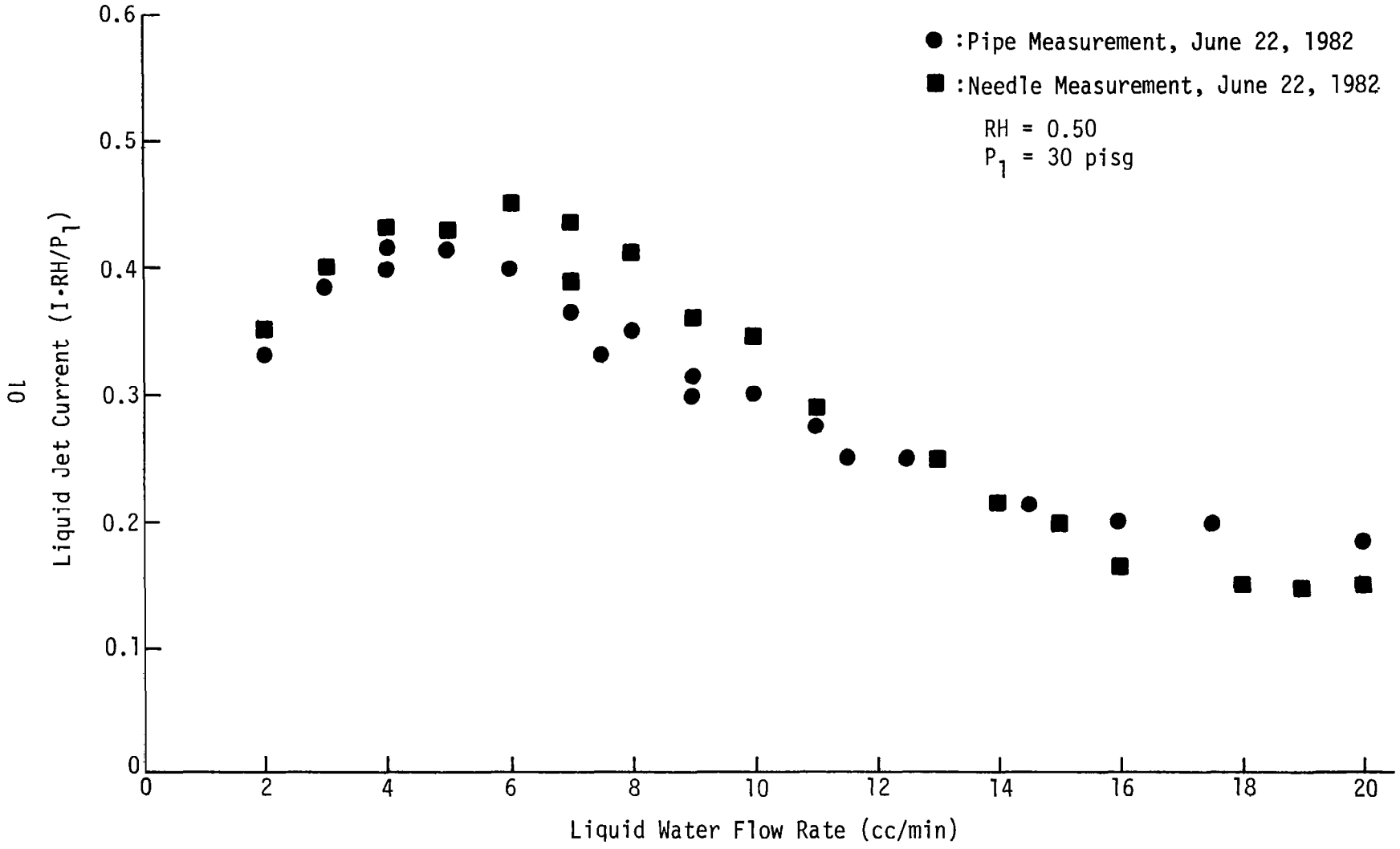

Figure 3.2 Comparison of the variation of scaled current output versus liquid water flow rate with two different measurement techniques.

control settings. The bottom of the pipe and the needle were placed 1/2 inch above the plane of the nozzle exit. Both systems measured essentially the same values. Any difference is attributed to experiment variability.

The optimum current output occurs at a liquid water flow rate in the range of 4 to 7 cc/min. Figure 3.3 compares the recent results with previous measurements. Both recent and previous results agree reasonably well. The scatter in the data is again attributed to experiment variability; particularly in view of the difficulty associated with maintaining a stable water flow rate in previous tests.

3.1.2 Corona Voltage

The circuit for measuring the corona voltage is shown in Figure 2.3. Figure 3.4 shows the measured variation of jet current output with the corona voltage. The output current is roughly proportional to the corona voltage over the range 4 to 12 kV. Generally, the voltage drop across the gap between attractor and the needle was not stable. This was due to the natural unsteady nature of a corona discharge (Loeb 1965). Also, the turbulent flow in the nozzle vibrates the needle and changes the electrical field of the corona, causing a corresponding change in the output current.

3.1.3 Vertical Variation of Current in Air Jet

The vertical variation of electrical current in the air jet was measured by moving the needle probe and pipe vertically. Figure 3.5 shows the results of both the needle probe and pipe measurements. Again, there is no apparent difference. Figure 3.6 shows the comparison of the recent results and previous results. The recent results appear to be roughly 20 percent higher than the previous results measured with the needle. No effort to scale these results has been made. Note, however, the scaling in Figure 3.3 tends to collapse the data onto one curve. Other differences may be due to experimental variability for each run caused by small changes in the position of the needle relative to the attractor, for example, and by variation in cleanness of the air filter, etc. Variation of current with height results from charges

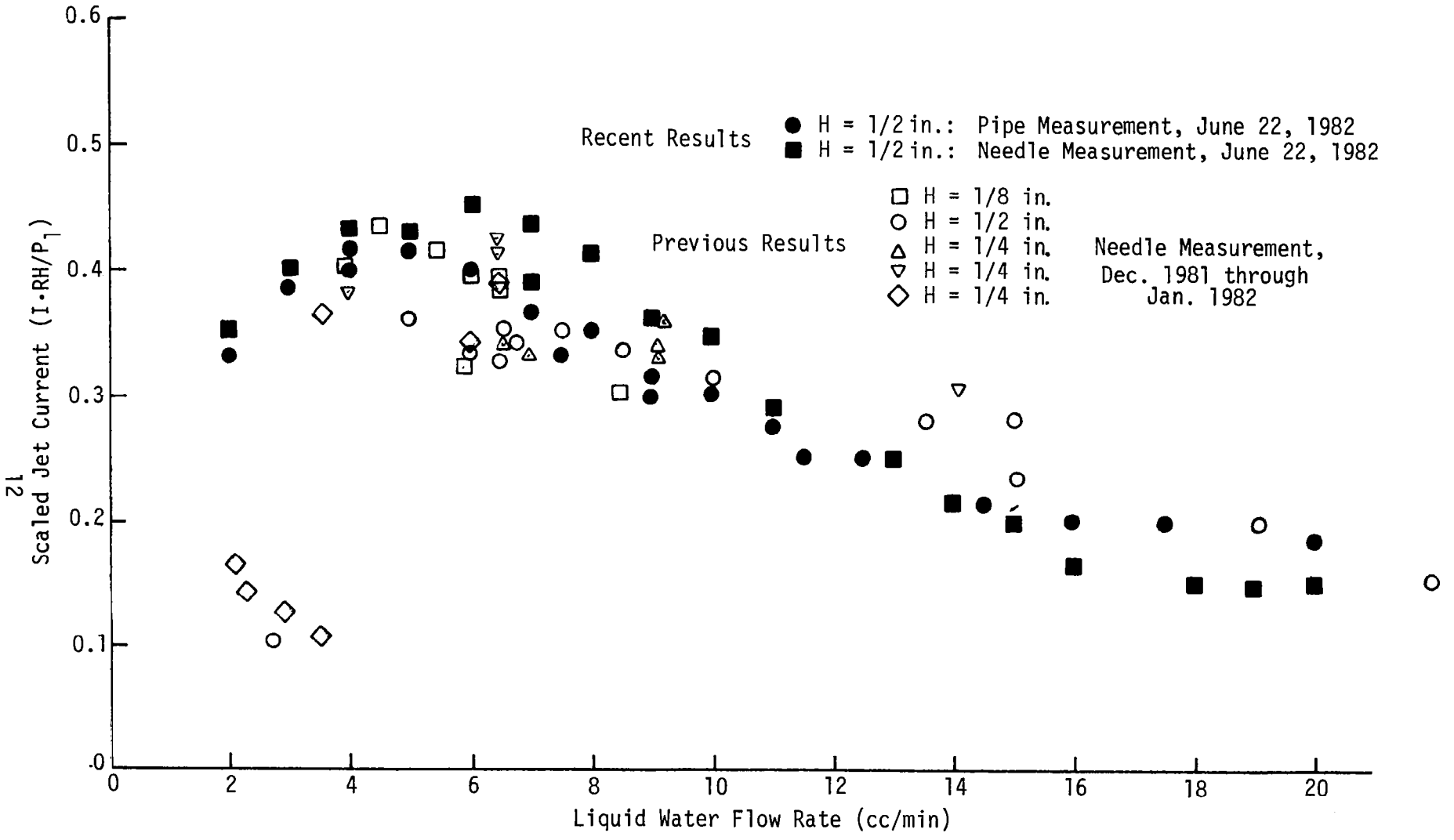

Figure 3.3 Comparison of the scaled current output from recent results with previously measured values. (H = height above the exit plane of the nozzle.)

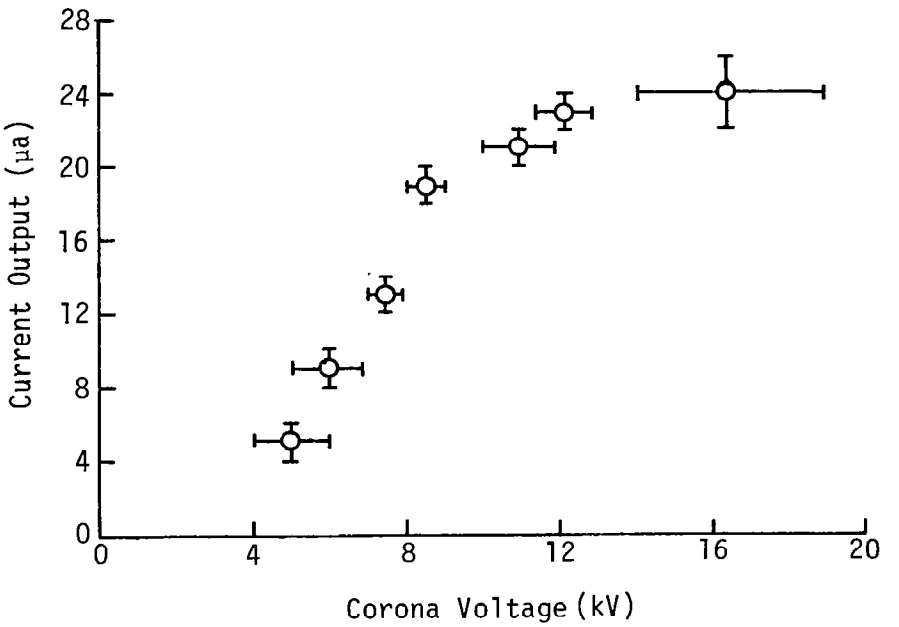

Figure 3.4 Variation in jet current output with corona voltage.

migrating out of the jet due to turbulence and their own mobility in an electric field.

3.2 Voltage Potential Distribution

The variation of voltage potential along the air jet was measured by adjusting the needle probe vertically and connecting the needle probe in series with the high-voltage probe and digital voltmeter, as shown in Figure 3.7. Figure 3.8 shows the measured vertical voltage distribution in the air jet for two different values of the corona supply voltage. The trend of both sets of data are the same. The voltage potential increased from the exit of the nozzle and reached a maximum at 2 to 3 inches above the exit and then decreased gradually.

The peak in the voltage distribution in the vertical direction is associated with the point where the kinetic energy of the droplets issuing from the nozzle is converted to electrical potential energy. Above the height at which the peak voltage occurs, the charged droplets are displaced upwards due to their mutual repulsion.

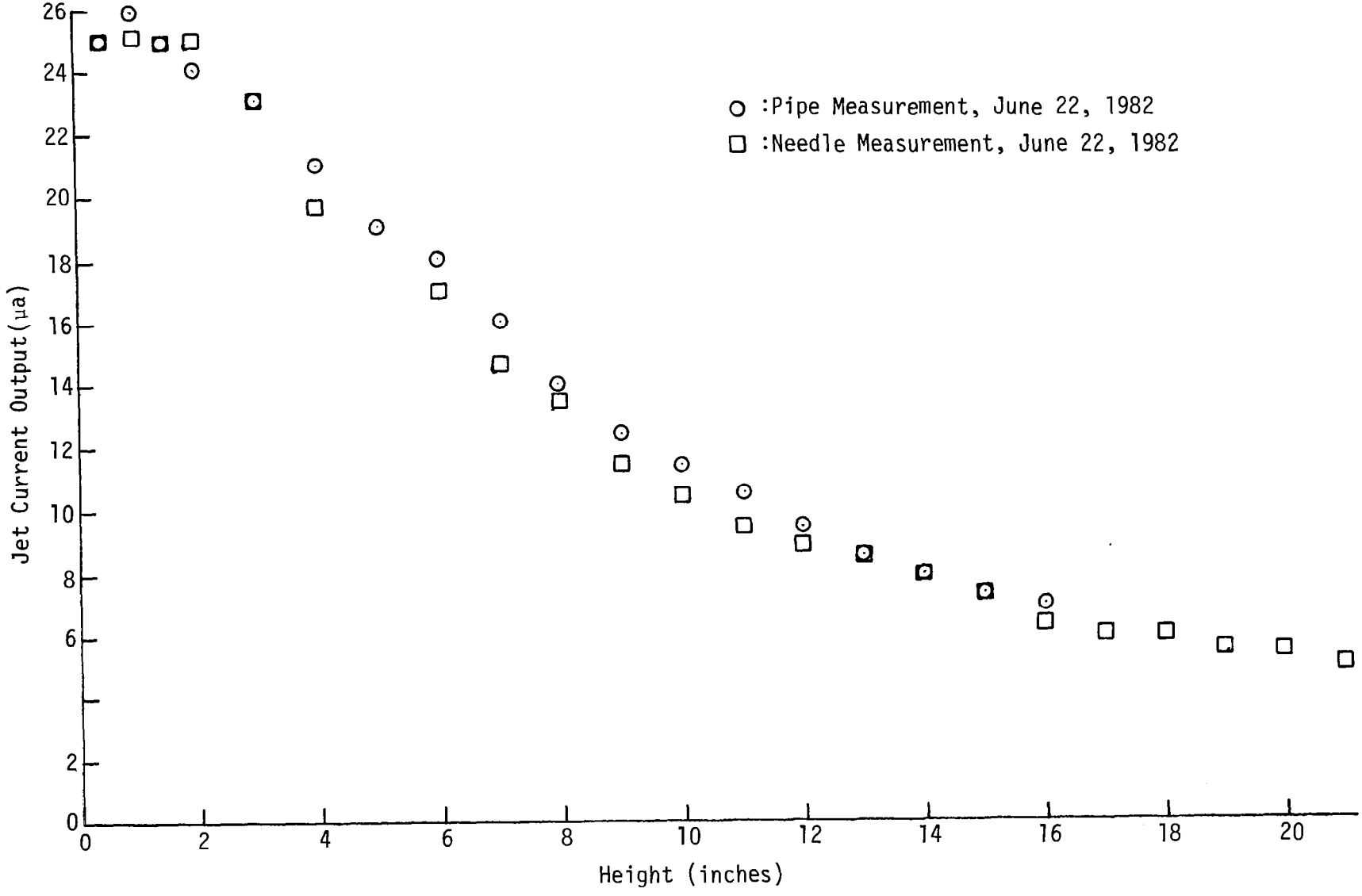

Figure 3.5 Comparison of the jet current versus height above exit plane of the nozzle for the two different measuring techniques.

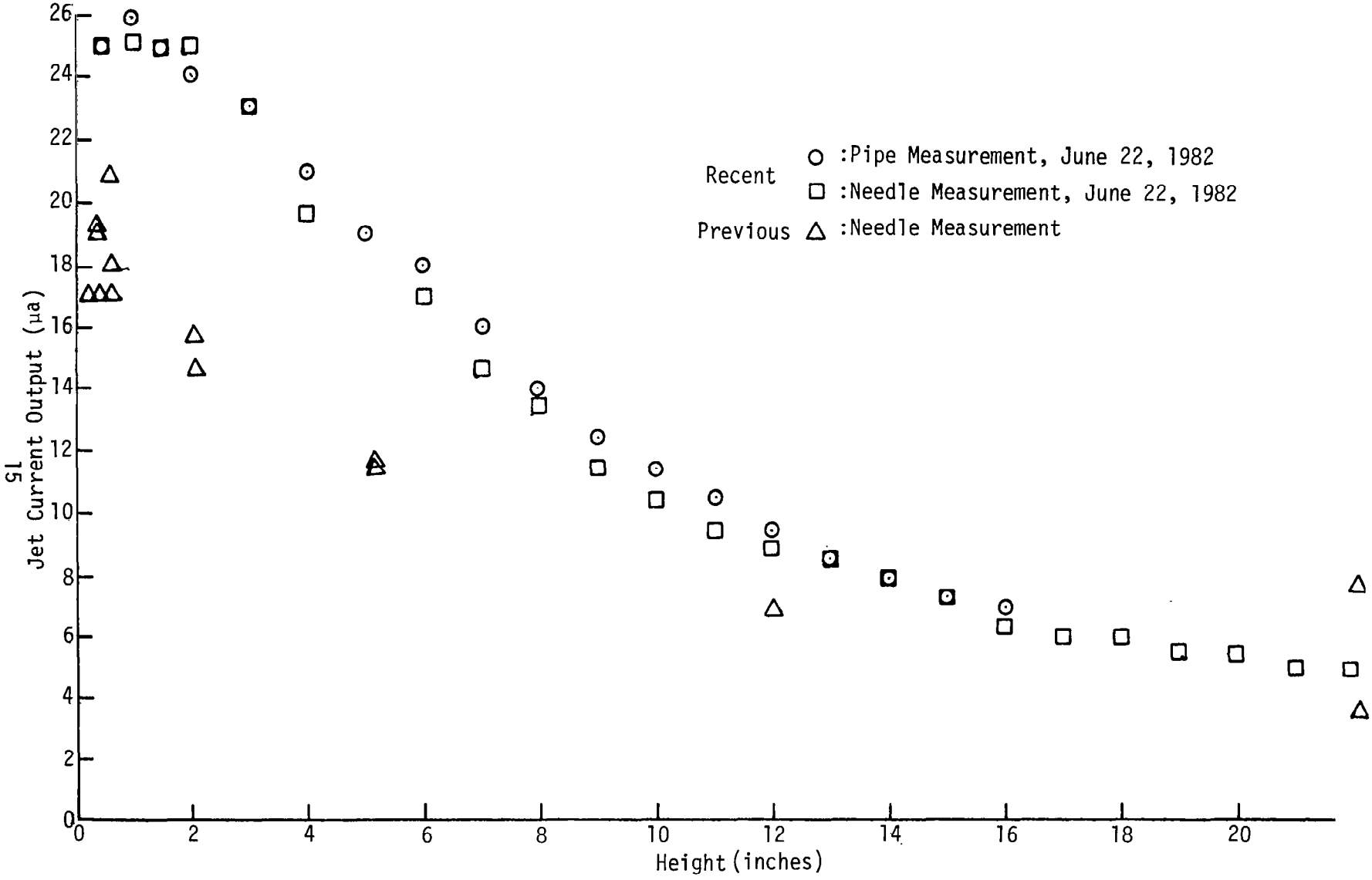

Figure 3.6 Comparison of the measured current output versus height above the exit plane of the nozzle with previous measurements (Frost 1982).

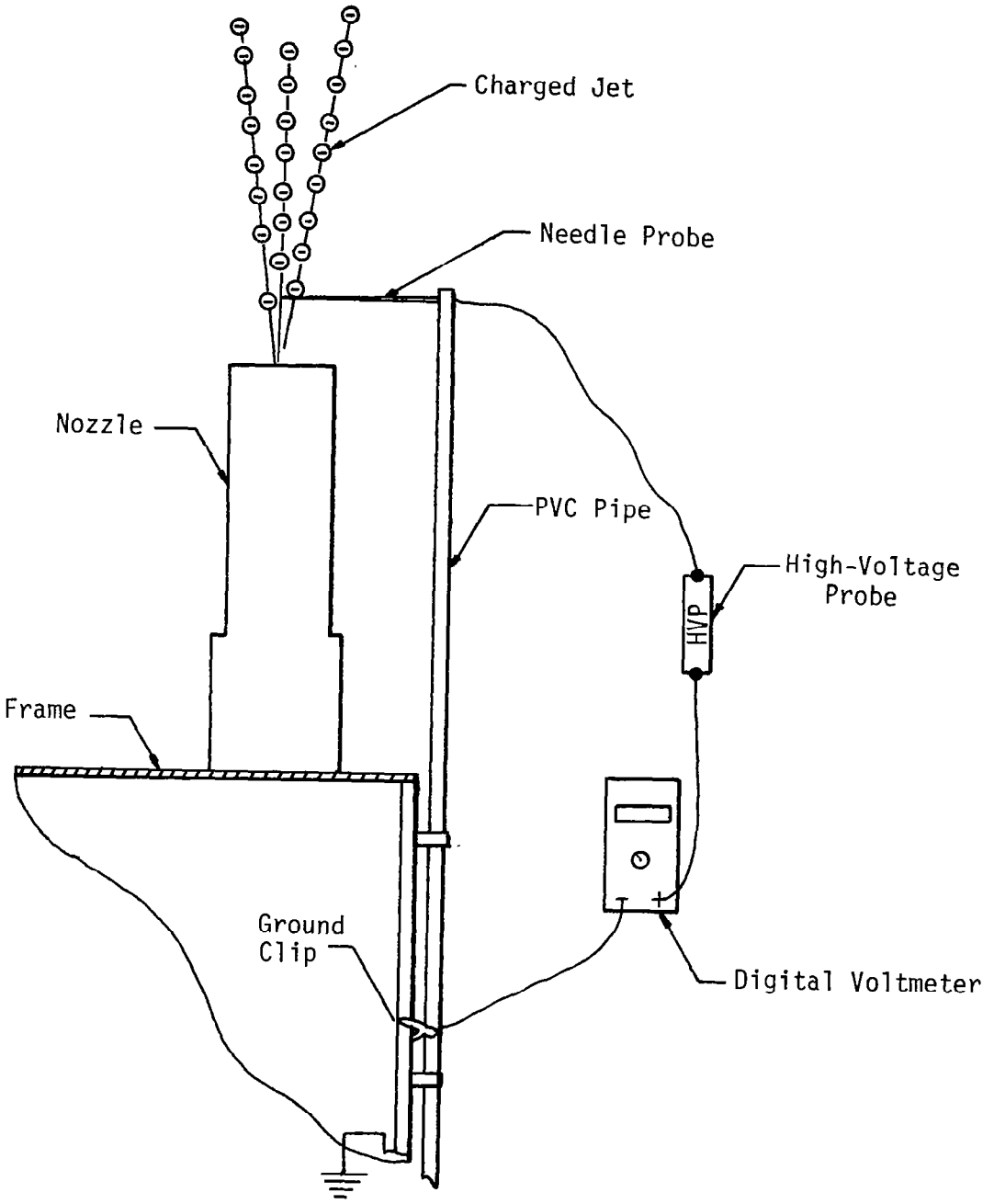

Figure 3.7 Illustration of jet voltage measurement.

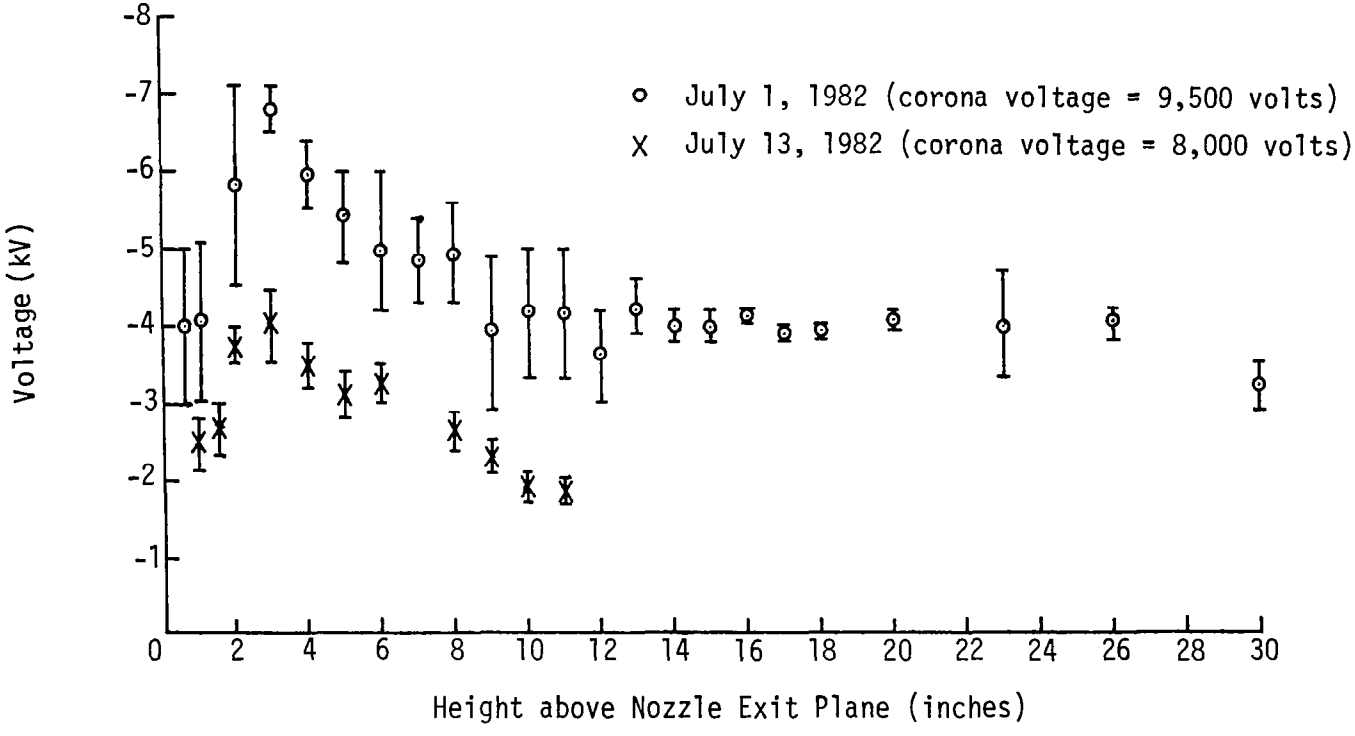

Figure 3.8 Vertical variation of voltage along the charged air jet (water flow rate $\dot{m}$ = 6 cc/min).

Ruhnke (1970) carried out a computer analysis where he solved both the Poisson electric field equation and the continuity equation for current. Figure 3.9 is a plot of his numerical results. The data measured in these tests are compared with the theoretical model by scaling the voltage with the maximum voltage and the height with the height at which the maximum voltage occurs, z_m. Figure 3.10 compares the measured data with the numerical results. The experimental data are found to bracket the analytical results very well.

3.3 Velocity Distribution in Air Jet

A pitot tube was used to measure the jet velocity in both the vertical and radial directions. The ALNOR† 6000-P velocimeter, which is generally used for measuring low-speed channel flow velocities, was used for this purpose. The range of this pitot tube is only 0 to 10,000 fpm (0 to 50.8 m/s). Thus, the meter read off-scale when measuring the jet flow velocity from the exit of the nozzle to approximately 10 inches above the plane of the nozzle. Above this height the meter provided meaningful results. Figure 3.11 shows the measured vertical velocity profiles at different heights above the nozzle exit plane. While the measured data is rather rough because of the crosswind effect, the trends of the distributions are clearly indicated. As expected, the velocity profile is sharper and narrower at lower levels and flatter and wider at higher levels. Figure 3.12 shows the variation of the centerline velocity of the jet with height. Again, the data is measured only at heights above 10 inches from the jet exit plane.

Measurements of the jet velocity were compared with theoretical models and other empirical models reported in Rajaratnam (1976). Rajaratnam predicts that the velocity along the centerline of the jet scaled with the velocity at the jet exit varies inversely with the distance along the jet scaled with the jet diameter. However, the axial decay of the velocity for circular jets in cross flow, as predicted

---

†Trade name of Alnor Instrument Company, 7301 North Caldwell Avenue, Niles, IL 60648.

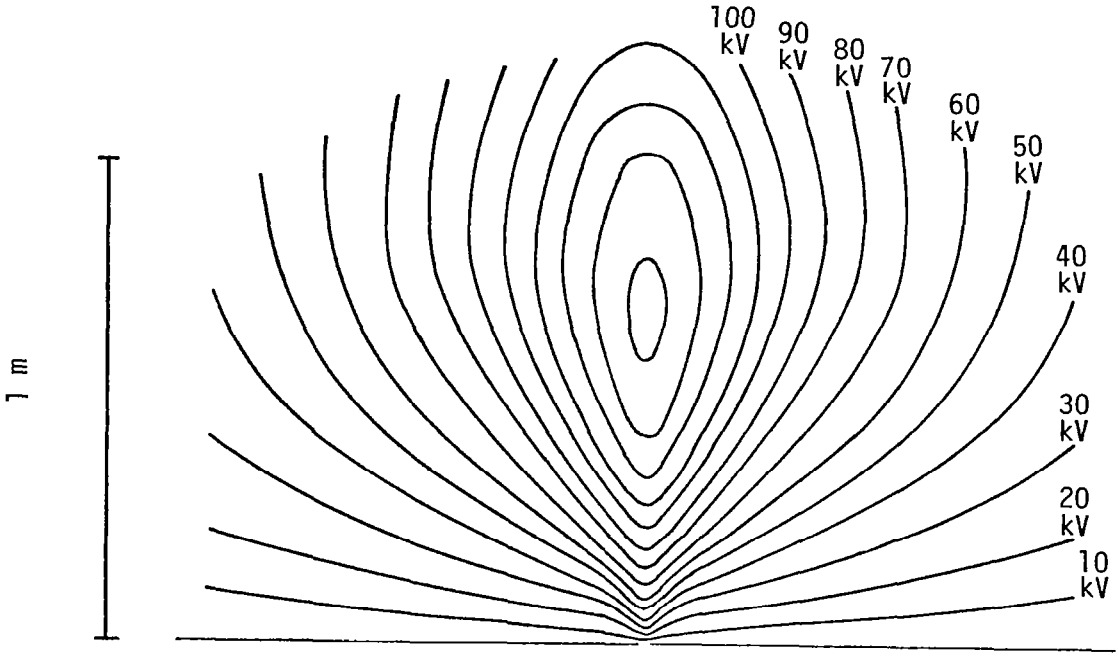

Figure 3.9 Computed voltage potential distribution in a space charge jet (Ruhnke 1979).

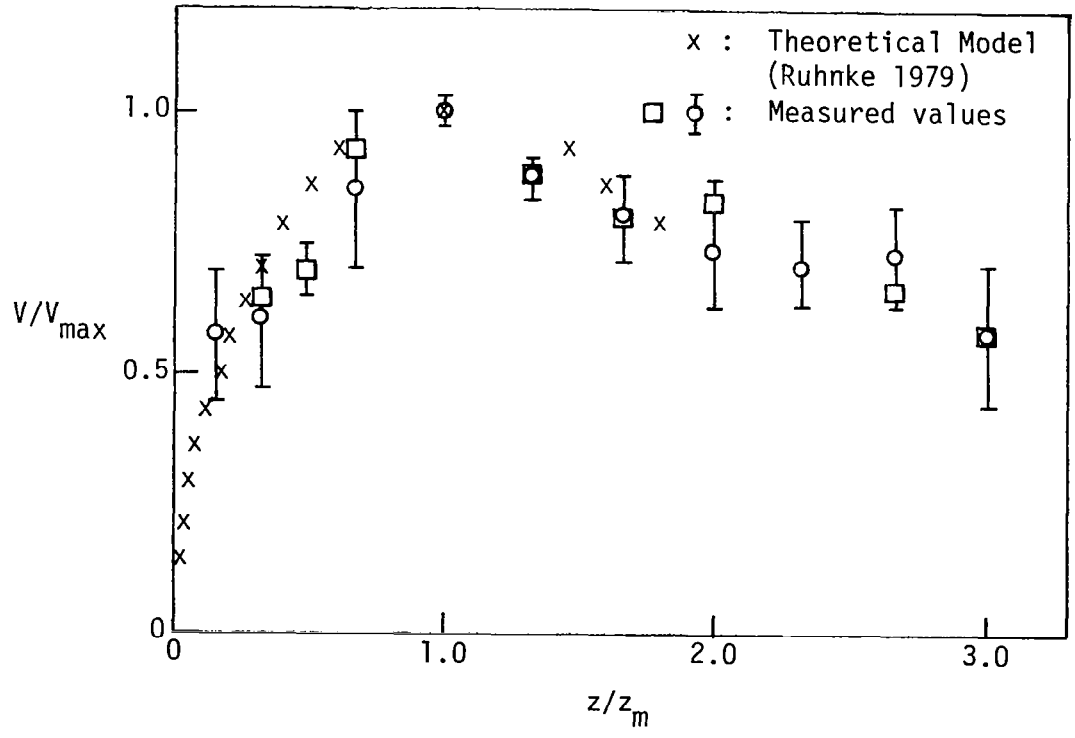

Figure 3.10 Comparison of scaled measured data and numerical predictions (Ruhnke 1979). (z_m = height above nozzle exit plane where voltage is maximum.)

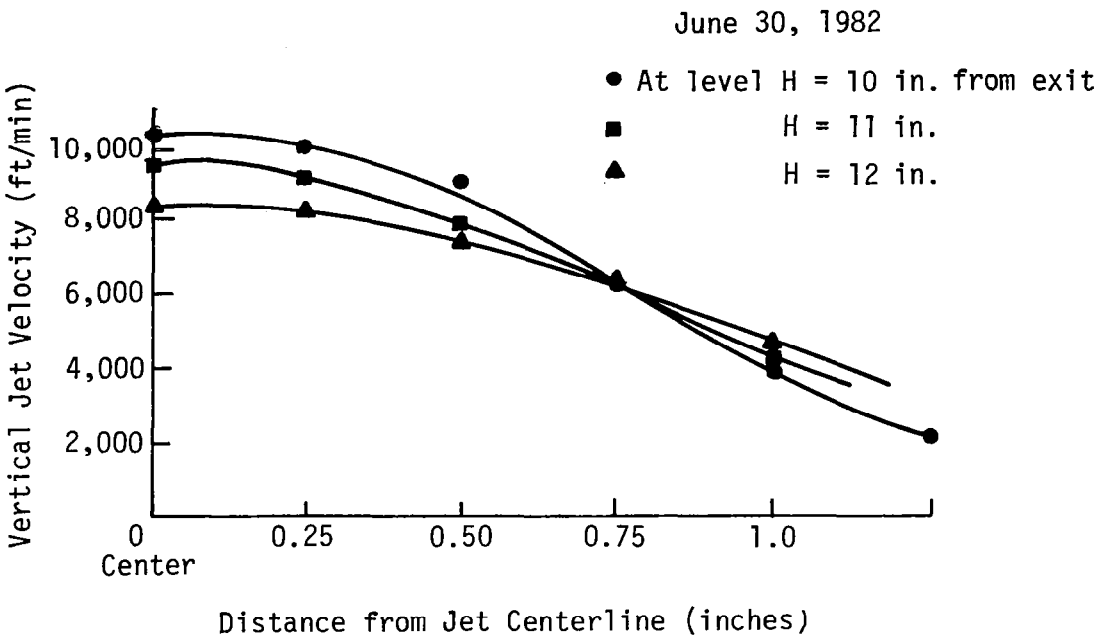

Figure 3.11 Radial velocity across the jet at different levels.

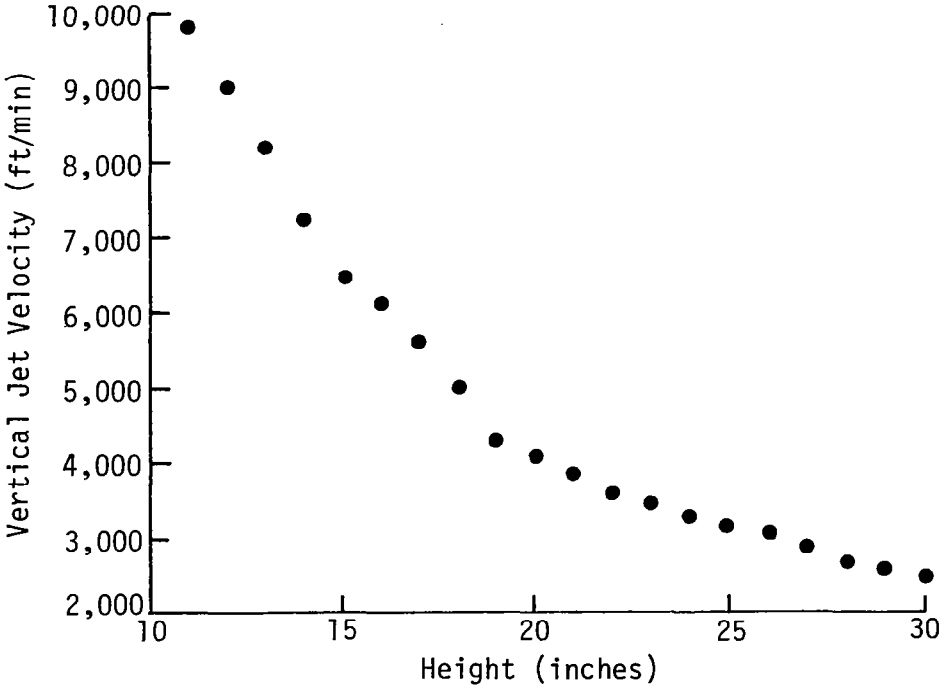

Figure 3.12 Velocity at center of jet versus height above the plane of the nozzle exit.

by Patrick (1967), is illustrated in the insert of Figure 3.13. The measured data shown in Figure 3.13, similarly scaled, clearly illustrates the same behavior as that of the circular jet in cross flow.

For working purposes, an empirical curve fit of the data was computed as shown in Figure 3.14. The scaled velocity is found to correlate roughly with $z/d_o^{-1.5}$. The results of comparing the measured jet velocity with previous experimental correlations is believed to indicate that the velocity measurements, although relatively crude, provide meaningful results.

3.4 New Nozzle Evaluation

The new nozzle was cast with the attractor at the throat because it was anticipated that condensation occurred at that location. Unfortunately, there were some defects in the new nozzle. Without the needle blockage at the throat, the throat area was now too large for the 15 SCFM compressor to provide sufficient flow to achieve choked conditions. Thus, Mach 1.00 at the throat did not occur, greatly reducing any droplet condensation which might occur there (Wegener and Mack 1958). The attractor and electrical lead were not properly sealed to the casting with the result that there was flow leakage through the gap between the electrical lead and the Plexiglas. At high corona voltages, severe arcing occurred at this spot and resulted in burning of the wire insulation, compounding the problem. Eventually the nozzle could no longer be used.

The new nozzle was tested but did not perform as expected because of the above-mentioned difficulties. The maximum stagnation pressure was 24 psig with the pressure regulator completely opened. Higher pressure could not be reached because the compressor could not supply a higher flow rate. Under these airflow conditions, the output current was only 8 μa when the rheostat was set to approximately 8,000 volts.

The new nozzle thus provided little (some quantitative effects were observed but the evidence is weak and they will not be discussed at this time) if any useful data. Consequently, all reported results are for tests carried out with the old nozzle.

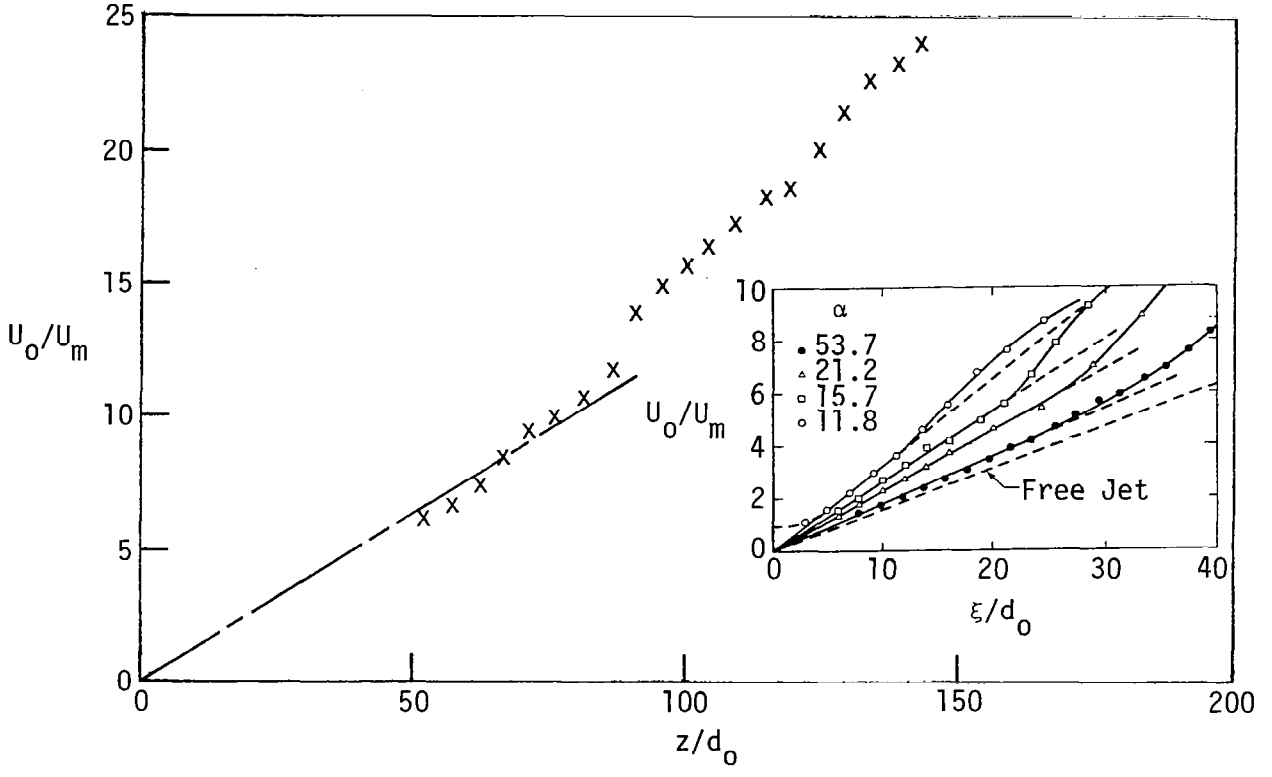

Figure 3.13 Measured axial decay of scaled velocity (insert from Patrick 1967). (ξ = curved distance along the jet centerline.)

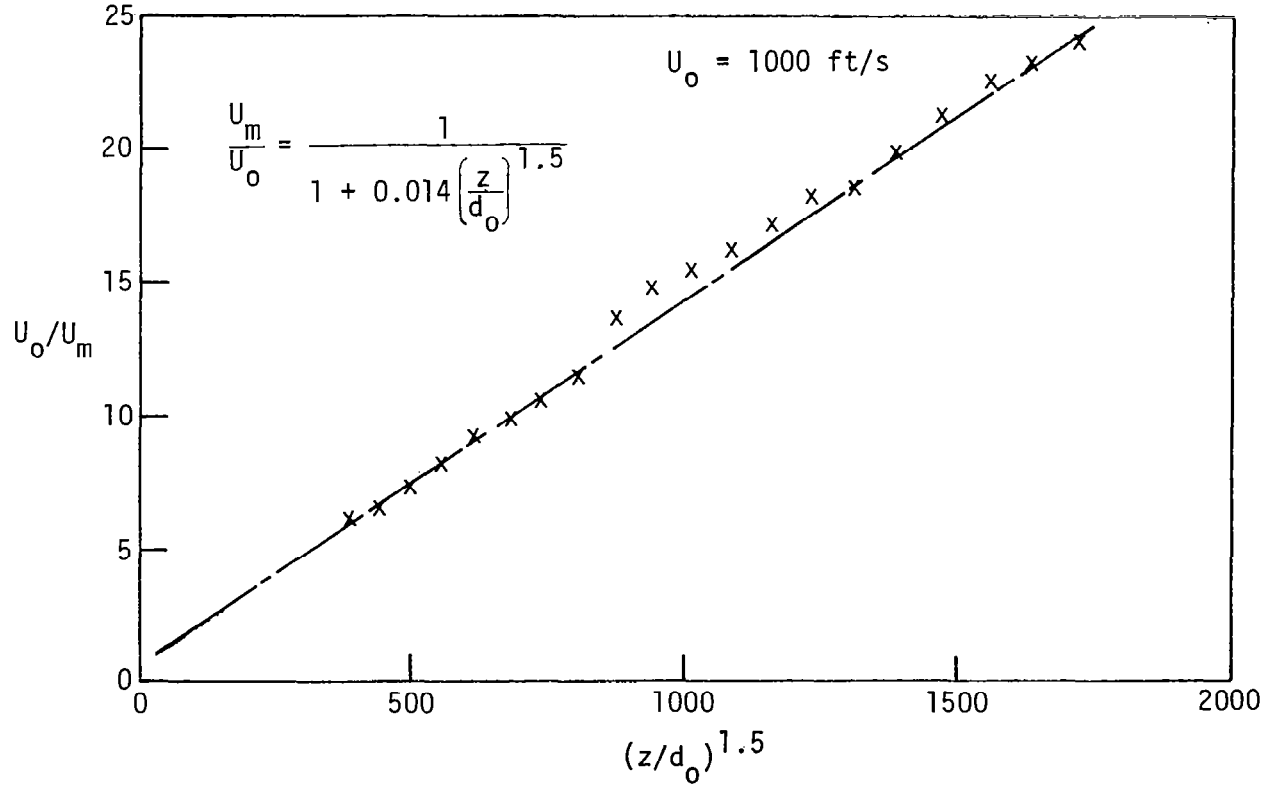

Figure 3.14 Curve fit on measured centerline jet velocity versus height above nozzle exit plane.

To correct the above-noted deficiencies in the nozzle, it is necessary to machine a new centerpiece for the mold used to cast the nozzle. The machining of the centerpiece is quite intricate and will be relatively expensive. To improve the seal between the attractor wire and the casting, it will be necessary to pour a new casting. This is not expensive, but time-consuming. Casting of the nozzle is not routine but requires some artistry. It is believed, however, that this will not create a problem in mass production of the electric charged particle generators since, for this operation, a production-type mold and casting procedure will be developed.

4.0 CONCLUSIONS

The results of the experiment carried out in this study indicate that a charged particle generator, which will routinely generate an output current of 20 μa or greater, can be constructed and will operate consistently. Conclusions from the experiment relative to the proposed nozzle modifications were not reached because of defects in the nozzle which could not be overcome within the time frame of the study. The addition of a positive displacement pump to supply the liquid water to the atomizer valve proved highly successful. With this new arrangement, the charged particle generator, using the old nozzle, ran continuously without adjustments to the controls. Other conclusions reached during the study are as follows.

1. Measurements of the jet output current using both the cylindrical pipe collector and the needle probe arrangement showed identical results within the variability of the experiment. It is concluded, therefore, that all previous measurements using a needle probe are meaningful and that the measured variation of electric current output with height along the centerline of the jet and as a function of the liquid water supply are true measures of the charged particle generator output capabilities.

   Additionally, measurements of the voltage using a special high-voltage probe show the experimental data to behave in accordance with theoretical analyses based on numerical solutions of a simple turbulent jet flow model with the Poisson field equation and continuity of current.

2. Measured velocities along the centerline of the jet compare well with other reported experimental results obtained in the laboratory and from theoretical analyses. The empirical curve fit of the centerline velocity provides a useful working equation for analyzing the ability of the jet to disburse charged particles to given height as described in Appendix B.

3. Measurements of the corona voltage drop versus the output current from the jet show a roughly linear relationship from 4 to 12 kV.

Based on the measured results, an estimate of the size of the charged water droplets can be made. This analysis is given in Appendix C. The results indicate that the droplet size lies in the range of 0.8 to 0.4 μ.

The charge to mass ratio computed for the prototype generator, i.e., output current divided by liquid water flow rate, gives an estimated result of 0.2 to 0.3 couls/kg. Lapple (1972) indicates that the range of charge to mass ratio achieved with a needle/attractor system as employed in this study is from 0.01 to 5 couls/kg. This observation is consistent with the measured results.

REFERENCES

Crawford, Martin (1976): Air Pollution Control Theory. New York: McGraw-Hill, pp. 298-361.

Frost, Walter (1982): Preliminary Test Results of Electrical Charged Particle Generator for Application to Fog Dispersal, Final report on Contract NAS8-33541, by FWG Associates, Inc., Tullahoma, TN 37388, for NASA Marshall Space Flight Center, AL 35812.

Frost, Walter, and Huang, Kao-Huah (1982): Bimonthly report on NASA Contract NAS8-34729, by FWG Associates, Inc., Tullahoma, TN 37388.

Frost, Walter, Collins, Frank G., and Koepf, David (1981): Charged Particle Concepts for Fog Dispersion, NASA CR 3440.

Lapple, C. E. (1972): Electrostatic Phenomena with Particulates, Advances in Chemical Engineering. New York: Academic Press, pp. 1-96.

Loeb, L. B. (1965): Electrical Coronas; Their Basic Physical Mechanics. Los Angeles: University of California Press.

Loveland, R. B., et al. (1972): Project Foggy Cloud IV, Phase II--Warm Fog Modifications by Electrostatically Charged Particles, Naval Weapons Center, China Lake, Calif.

Patrick, M. A. (1967): Experimental Investigation of the Mixing and Penetration of a Round Turbulent Jet Injected Perpendicularly into a Transverse Stream, Trans. Inst. Chem. Eng., 45:T16-T31.

Rajaratnam, N. (1976): Turbulent Jets. New York: Elsevier Scientific Publishing Company.

Ruhnke, Lothar H. (1979): Personal communications.

Ruhnke, Lothar H. (1970): Warm Fog Modification by Seeding with Unipolar Ions, Preprint of paper presented at the American Meteorological Society Second National Conference on Weather Modification, April 6-9, Santa Barbara, Calif.

Schultz, R. D., and Branson, L. (1959): The Colloid Rocket: Progress Towards a Charged-Liquid-Colloid Propulsion System, Paper presented at the Second Symposium on Advanced Propulsion Concepts, Boston, Mass.

Schultz, R. D., and Weich, R. E. (1960): Electrical Propulsion with Colloidal Materials, AGARD Combustion and Propulsion Panel Technical Meeting on Advanced Propulsion Concepts, Pasadena, Calif.

Wegener, P. P., and Mack, L. M. (1958): Condensation in Supersonic and Hypersonic Wind Tunnels, Advances in Applied Mechanics, Vol. 5, H. L. Dryden and T. von Karman (editors). New York: Academic Press.

APPENDIX A

SPECIFICATIONS OF HIGH-VOLTAGE PROBE

The B & K-Precision high-voltage probe is a self-contained range multiplier designed to extend the voltage range of any constant input impedance type voltmeter. It is particularly suited for use with the following B & K-Precision instruments:

MODEL NO.			
277	282	2800	2830
280	283	2810	
281	290	2815	

The outside case is made of high-impact ABS type plastic, which insures excellent insulation, impact resistance, and light weight.

SPECIFICATIONS

Voltage Range:	Usable to 40 kV DC. Multiplies instrument range by 1000. (E.g., 50V becomes 50,000V). May be used with any instrument having a constant input impedance of 10 or 15 megohms.
Impedance:	600 megohms nominal.
Accuracy:	±3%, plus instrument accuracy.
Calibration:	Internal; factory calibrated at 25 kV.
Frequency Range:	DC to 80 Hz.

IMPORTANCE OF MEASURING THE HIGH VOLTAGE

All color TV sets require a specified value of high voltage If the high voltage is incorrect, the set may not function properly. Before any color set can be accurately converged, the high voltage must be checked and/or adjusted to the manufacturer's specifications.

A second reason for checking the high voltage arises from the possibility of X-ray radiation from certain sets, particularly older models. The possibility of this hazard is increased if the high voltage of the receiver is excessive. Always check the manufacturer's instructions and specifications prior to performing high-voltage measurements.

APPENDIX B

PREDICTION OF CHARGED PARTICLE TRAJECTORY

The motion of a charged particle in a jet is governed by the drag due to the jet flow, the electrical field, and the gravitational field. Based on the assumption that the temperature, density, gravity, and number of charges on the particle are constant, the equations of motion in Cartesian coordinates gives:

$$m\ddot{x} = -\frac{1}{2}\rho_a A C_D(\dot{x} - W_x)|V_a| + F_{ex}$$

$$m\ddot{y} = -\frac{1}{2}\rho_a A C_D(\dot{y} - W_y)|V_a| + F_{ey} \qquad \text{(B.1)}$$

$$m\ddot{z} = -\frac{1}{2}\rho_a A C_D(\dot{z} - W_z)|V_a| + F_{ez} - mg$$

where m is the mass of the particle with cross sectional area A; $\ddot{x}$, $\ddot{y}$, $\ddot{z}$ are the particle accelerations in the x, y, and z directions, respectively; ρ_a is the air density; C_D is the drag coefficient defined as a function of Reynolds number; W_x, W_y, and W_z are the three instantaneous wind velocity components; $|V_a|$ is the magnitude of the particle velocity relative to the air; g is the acceleration of gravity; and F_{ex}, F_{ey}, and F_{ez} are the components of the electrical force.

The three instantaneous wind velocity components W_x, W_y, and W_z, which appear in Equation B.1, result from the air jet; this assumes no meteorological wind field. A free jet model from Rajaratnam (1976) is used in the model. Figure B.1 is a sketch of a circular turbulent jet. The axial velocity of the jet in the fully developed region is given by

$$u(r,z) = \frac{U_m}{1 + 0.125\ \xi^2} \qquad \text{(B.2)}$$

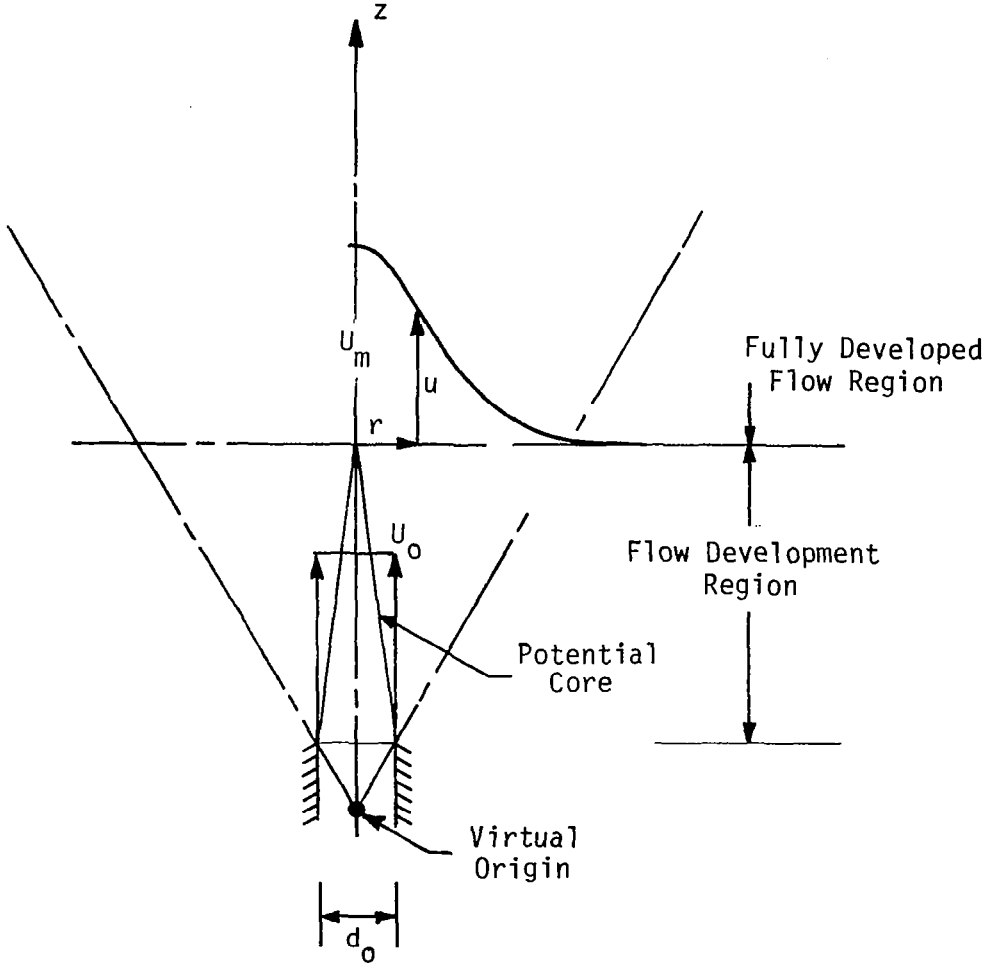

Figure B.1 Schematic and nomenclature for a circular jet (Rajaratnam 1976).

where $\xi = \sigma r/z$ and $\sigma = 18.5$ and the radial velocity is given by

$$v(r,z) = \frac{U_m(z)}{\sigma} \frac{\xi - 0.125\ \xi^3}{2(1 + 0.125\ \xi^2)^2} \tag{B.3}$$

The variation of the centerline velocity, $U_m(z)$, is shown in Figure 3.14, page 22. The curve fit is given by

$$U_m(z) = \frac{U_o}{1 + 0.014\left(\frac{z}{d_o}\right)^{1.5}} \tag{B.4}$$

where U_o is the nozzle exit velocity of the air jet. d_o is the diameter of the nozzle exit. Figure B.2 illustrates the axial velocity given by Equation B.4 at different heights.

In addition to the jet velocity field, the electrical field must be specified. The three components of the electrical field, F_{ex}, F_{ey}, and F_{ez}, in Equation B.1 can be expressed as

$$\begin{aligned} F_{ex} &= 1.6 \times 10^{-9}\ nE_x \\ F_{ey} &= 1.6 \times 10^{-9}\ nE_y \\ F_{ez} &= 1.6 \times 10^{-9}\ nE_z \end{aligned} \tag{B.5}$$

where n is the number of charges on each particle and E_x, E_y, and E_z are the three components of the electrical field vector. From Ruhnke's (1970) analysis, the voltage potential field is as shown in Figure 3.9, page 19. The comparison between measured data and Ruhnke's (1970) calculation is discussed on page 18 and is shown in Figure 3.10, page 19.

The electrical field strength along the center of the jet is plotted in Figure B.3. The data in Figure B.3 are interpolated from the results of Ruhnke's (1979) numerical analysis (see Figure 3.9). In Figure B.3 the electrical field strength is normalized by E(0), which is the strength

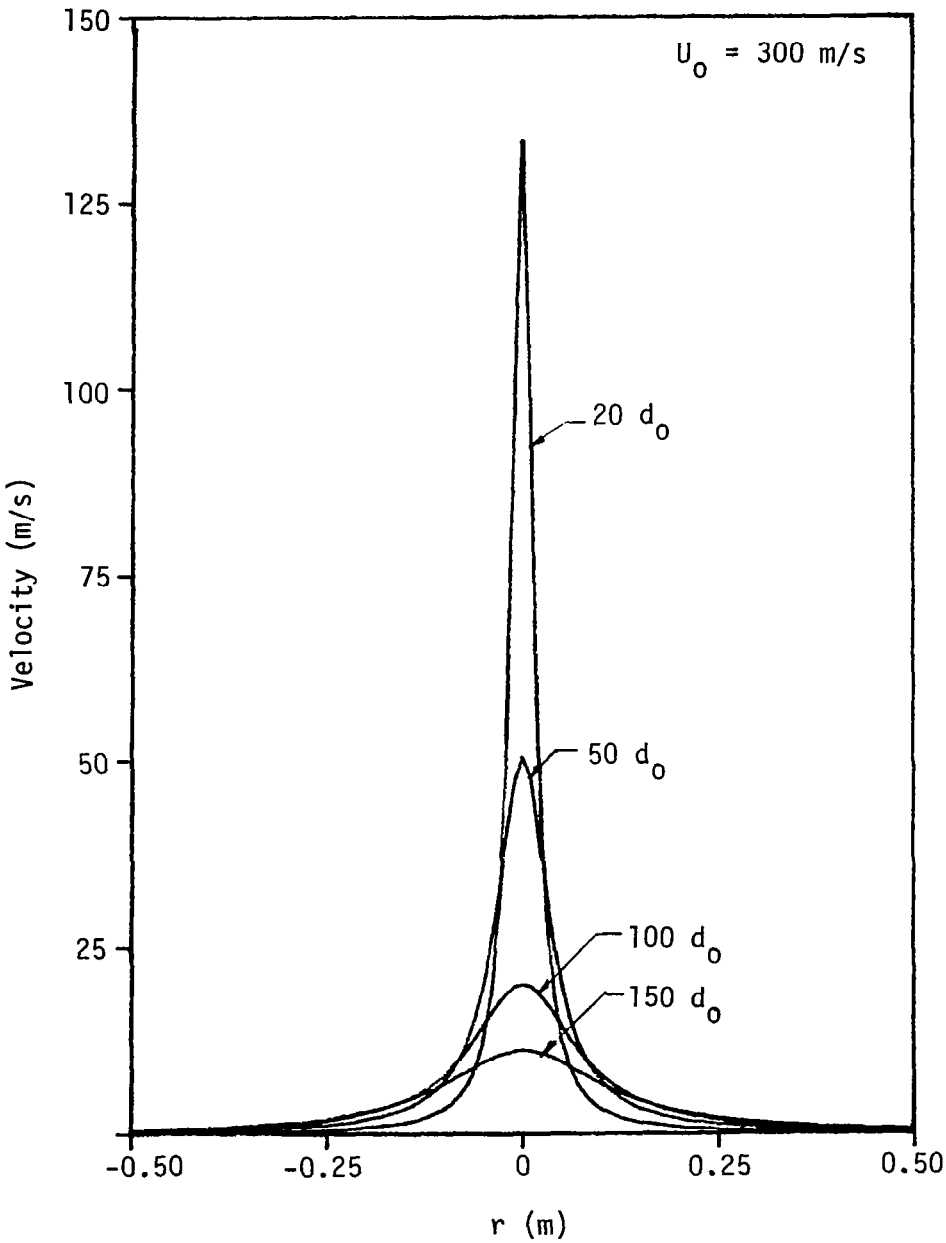

Figure B.2 Axial jet velocity at different heights (d_o = nozzle diameter).

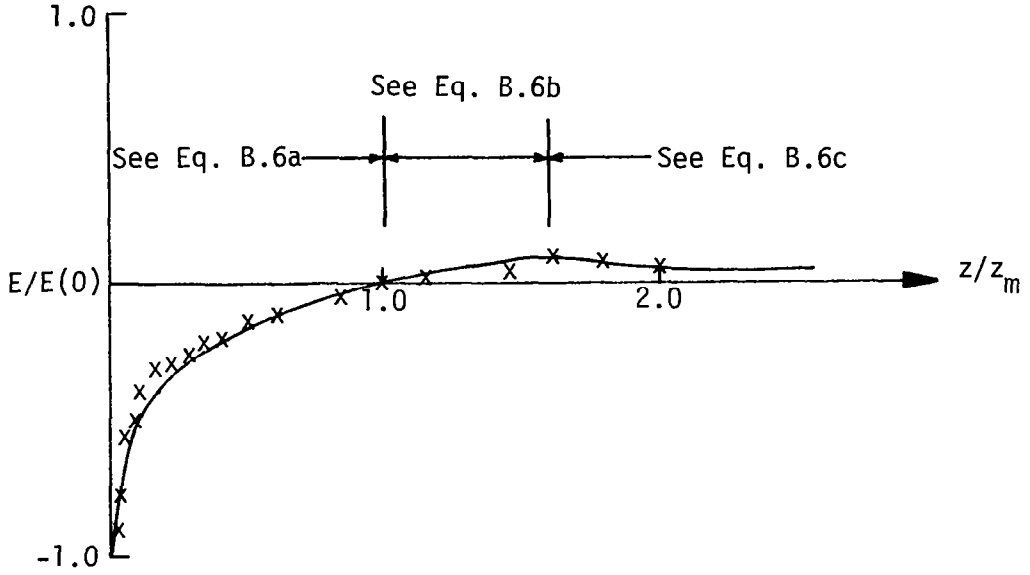

Figure B.3 Electrical field strength along centerline of vertical jet (z_m is the vertical distance from nozzle exit to where voltage is maximum).

at the nozzle exit. Also, the height is normalized by z_m, which is the vertical distance from the nozzle exit to the point where the magnitude of voltage potential is a maximum.

As Figure B.3 illustrates, the electrical field along the centerline of the jet can be divided into three regions. Curve fits of the electrical field for each region are

$$E(z) = \begin{cases} \dfrac{-10\ E(0)}{10 + (z/d_o)^2} \text{ when } z \leq z_m & \text{(B.6a)} \\ 0.1\ E(0)\ \dfrac{z - z_m}{0.6\ z_m} \text{ when } z_m < z \leq 1.6\ z_m & \text{(B.6b)} \\ \dfrac{0.1\ E(0)}{1 + z/z_m - 0.6} \text{ when } 1.6\ z_m < z & \text{(B.6c)} \end{cases}$$

The radial electrical field is given as (Frost et al. 1981)

$$E(r) = \begin{cases} \frac{r\rho_e}{2\varepsilon_o} \vec{r} \text{ when } r \leq R \\ \\ \frac{R^2\rho_e}{2r\varepsilon_o} \vec{r} \text{ when } r > R \end{cases} \tag{B.7}$$

where R is the radius where the radial electrical field is a maximum, $E_m(z)$. Equation B.7 can be rewritten as

$$E(z,r) = \begin{cases} \frac{r}{R} E_m(z) \text{ when } r \leq R \\ \\ \frac{E_m(z)}{r} \text{ when } r > R \end{cases} \tag{B.8}$$

R can be approximately expressed as a function of z by the relationship

$$R(z) = R_j + 0.333\ z \tag{B.9}$$

where R_j is the nozzle radius. Equation B.9 is estimated by interpolating the edges of the voltage field shown in Figure 3.9. The value of E_m is not constant in the jet field. The variation of E_m with height is shown in Figure B.4. Again, these data are based on Ruhnke's analysis. A two region curve fit gives

$$E_m(z) = \begin{cases} 10\ E_{rmax}\ (z/z_m)\ ;\ z \leq 0.1\ z_m \\ \\ \frac{E_{rmax}}{1 + \frac{2}{9}\ (z/z_m - 0.1)}\ ;\ 0.1\ z_m < z \end{cases} \tag{B.10}$$

where E_{rmax} is the maximum radial electrical field strength.

The expressions for electrical field strength (i.e., Equations B.10, B.8, B.6, and B.5) and for the wind field (i.e., Equations B.4, B.3, and B.2) are substituted into Equation B.1. Equation B.1 can be solved numerically, and the particle trajectories can be calculated based on given particle radius, jet exit velocity, U_o, and electrical field strength, E(0), and E_{rmax}.

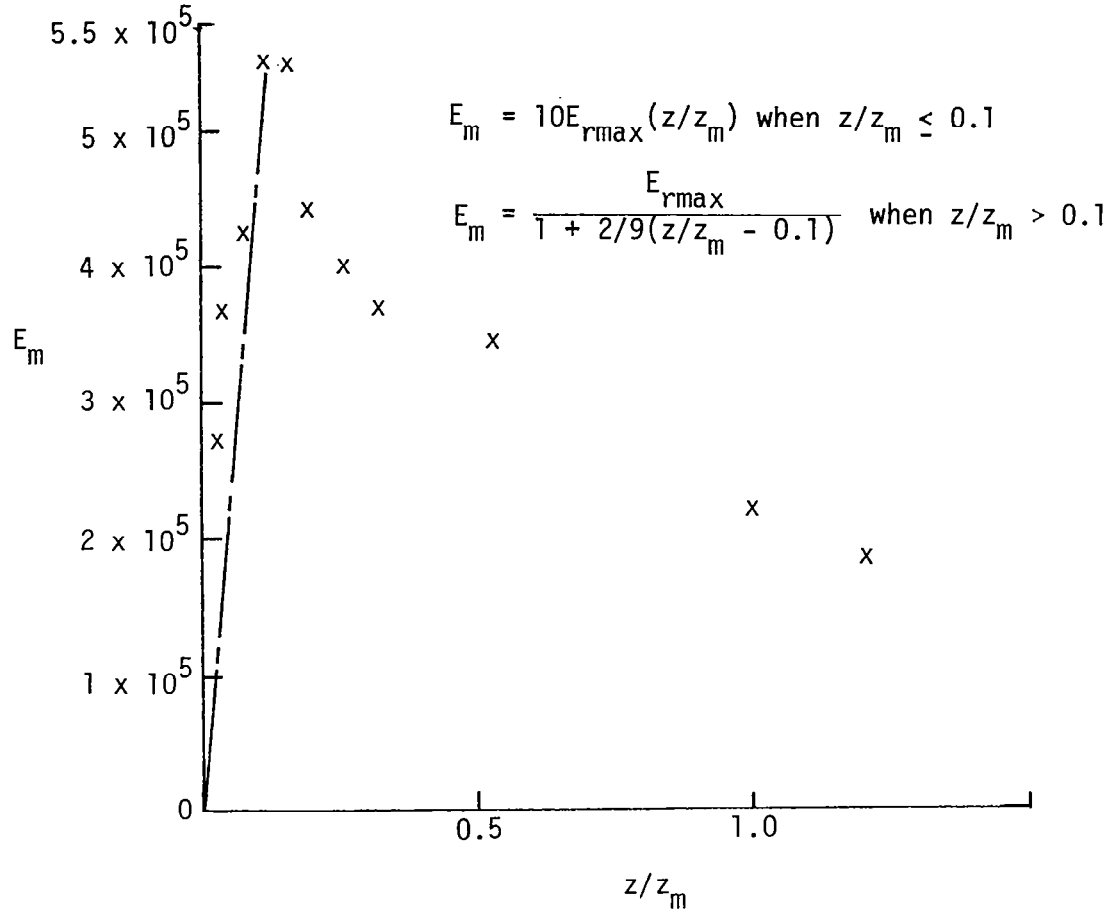

Figure B.4 Maximum radial electrical field strength along jet.

The input variables for solving Equation B.1 are based on the reported measured data. The electrical field strength at the nozzle exit E(0) is equal to 10^6 v/m. And the maximum radial electrical field strength, E_{rmax}, is estimated as 10^5 v/m. A uniform vertical electrical field of E = 100 v/m, which represents a fair-weather background, is assumed to exist. From Appendix C, the particle diameter d is estimated to be in the range from 0.4 to 0.8 μ. A value of d = 0.8 μ is used. The number of charges on each particle is equal to 327 e^- (this is the saturation charge). A nozzle exit velocity U_o = 300 m/s is also used. The computed particle trajectories based on the above data (which is representative of the current prototype charged particle generator system) are shown in Figure B.5. The origin of the particle trajectories are at the exit of the jet and at 0.001 m increments across the nozzle

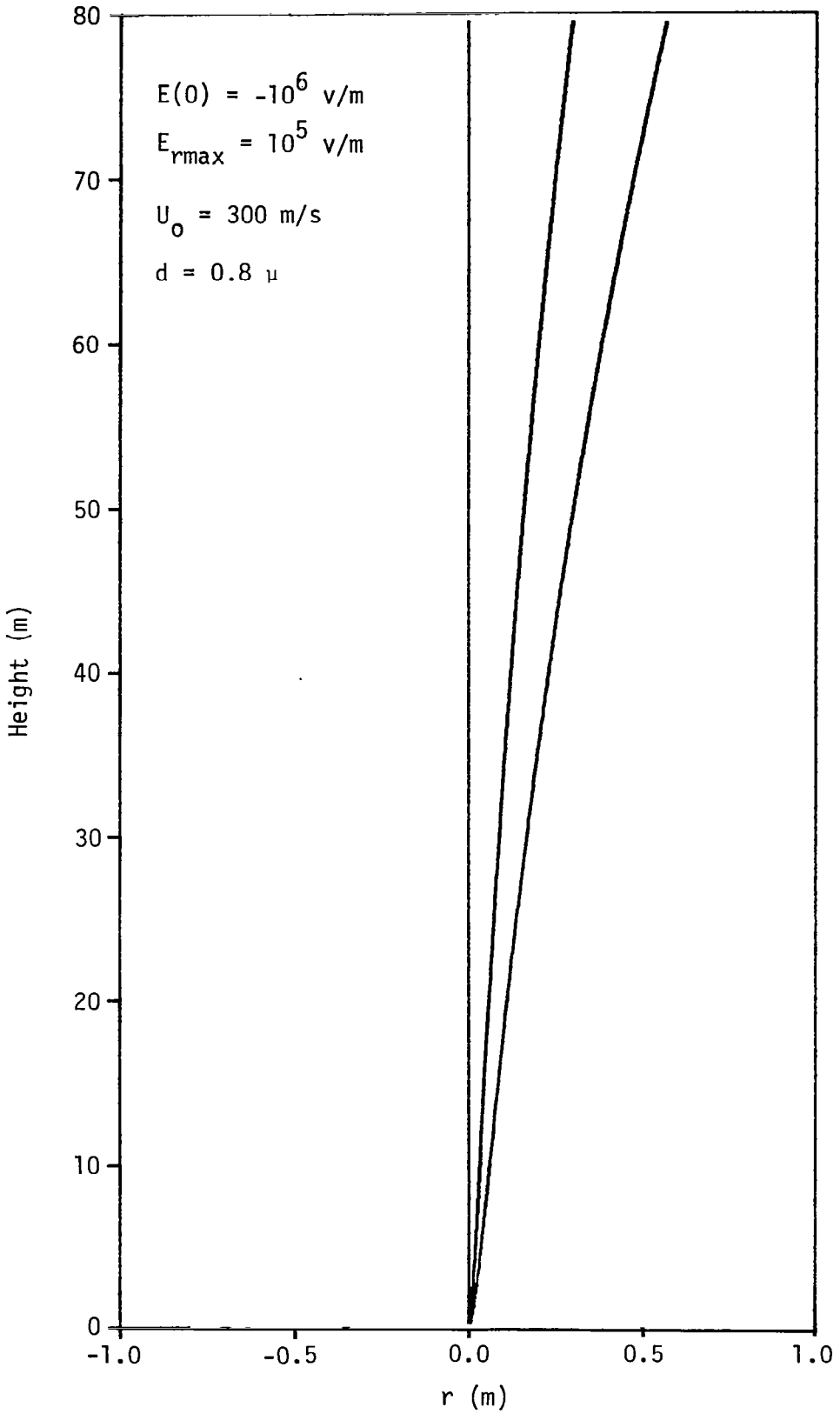

Figure B.5 Charged particle trajectories in a free jet with an induced electrical field.

exit, respectively. The figure shows that the 0.8 μ particle with saturation charge spreads outward to a distance on the order of 0.65 m and reaches heights of 80 m. Figure B.6 illustrates the computed particle trajectories in a free jet without an electrical field. Comparing Figures B.5 and B.6, the charged particles are seen to spread due to their electrical charge but not to exit the jet and return to ground as often hypothesized in the literature.

Realistically, the particle may not reach heights of 80 m because both the meteorological crosswind and the turbulent fluctuation in the jet are neglected. One can conclude qualitatively, however, that if the momentum of the jet flow can overcome the opposing electrical field (i.e., below z_m in Figure B.2) and thus push particles beyond z_m, the charged particle will then rise due to their induced field until the gravitational force becomes greater than the electrical force and the jet drag force.

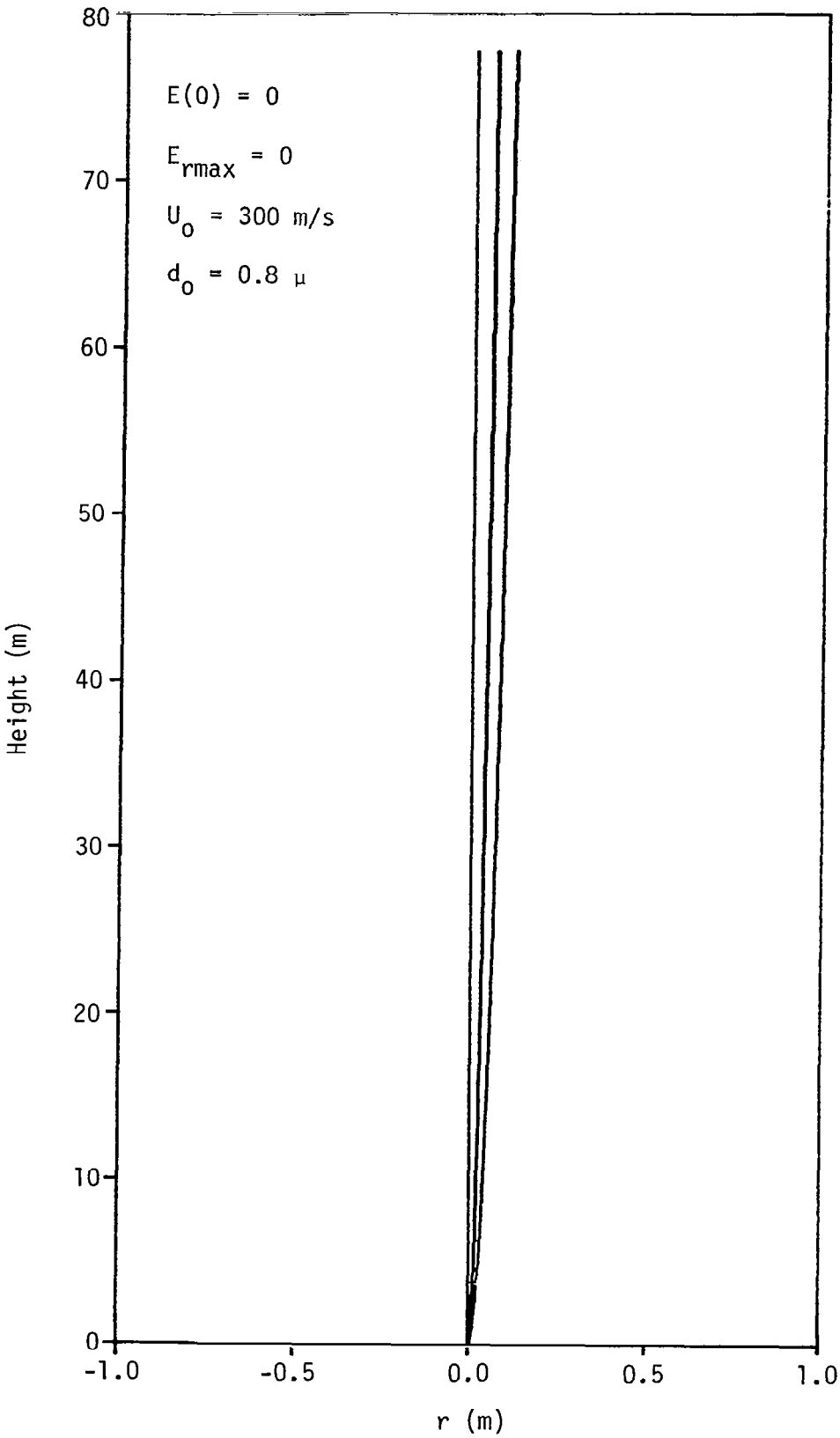

Figure B.6 Particle trajectories in a free jet without an electrical field.

APPENDIX C

ESTIMATE OF WATER DROPLET SIZE

The charge-to-mass ratio based on measured data is

$$\frac{C}{M} = \frac{20 \times 10^{-6} \text{ amp}}{(6 \text{ cc/min})(1/60 \text{ min/sec})(10^{-3} \text{ kg/cc})} = 0.2 \text{ coul/kg} \qquad (C.1)$$

The Rayleigh limit representing the maximum number of charges a droplet can acquire is given by

$$q_{ps} = 2.08 \times 10^{9} r^{2} E \text{ (for water droplets at 20° C)} \qquad (C.2)$$

This represents an upper limit on the amount of charge a droplet can obtain. From Equations C.1 and C.2 the radius can be computed for a given value of E_o.

The value of E_o, estimated from dividing the measured voltage drop across the corona by the separation distance between the needle and attractor, is roughly 10^6 v/m. Hence, the number of droplets per kilogram of water injected is

$$\frac{\text{Number of Particle}}{\text{Kilogram of Mass}} = \frac{1}{\left(\frac{4}{3}\pi r^3\right)\rho} = \#/\text{kg} \qquad (C.3)$$

The number of charges per particle becomes

$$\frac{\text{Number of Charge}}{\text{Particle}} = \frac{C}{M}\left(\frac{4}{3}\pi r^3 \rho\right) \qquad (C.4)$$

Equation C.4 must be less than or equal to the Rayleigh limit (i.e., Equation C.2). Hence,

$$(0.2 \text{ c/kg})\left(6.25 \times 10^{18} \frac{e^-}{c}\right)\left(\frac{4}{3}\pi r^3 \times 10^3\right) \leq 2.08 \times 10^{9} \times r^2 \times 10^{6}$$

The particle radius is therefore predicted to be on the order of r = 0.4×10^{-6} m or the diameter is d = 0.8 μ.

Since the droplet is only in the corona region a very short time, it may not be realistic to estimate the size of water droplets based on the Rayleigh limit. According to Crawford (1976), the rate of droplet charging in the corona is approximately

$$\frac{q_p}{q_{ps}} = \frac{t}{t_o + t} \tag{C.5}$$

where q_p is charges on the droplet and q_{ps} is saturation charge on the particle is given by Equation C.2. t_o is the time constant of this process defined as the value of t when $q_p = 0.5\ q_{ps}$. t_o is given by

$$t_o = \frac{4\varepsilon_o}{Nq_e k} \tag{C.6}$$

where N is ions density in the corona region, k is the mobility of the ions ($k = 2.2 \times 10^{-4}$ m^2/v s).

The charging time t is estimated by dividing the nozzle length with the airflow (essentially the droplet speed) velocity V, i.e.:

$$t = \frac{L}{V} \tag{C.7}$$

Introducing measured data into Equation C.7, t is found to be approximately 5.67×10^{-4} sec (V = 300 m/s is assumed). From Equation C.5

$$q_p/q_{ps} = 0.53$$

The ion density used in Equation C.6 was taken as $N = 2 \times 10^{15}$ ions/m^3 (see Crawford (1976)). q_{ps} is given by Equation C.2. Introducing $q_p = 0.53\ q_{ps}$, into Equation C.4, the droplet radius is found to be on the order of r = 0.2 μ or the diameter is d = 0.4 μ.

1. Report No.	2. Government Accession No.	3. Recipient's Catalog No.
NASA CR-3674		

4. Title and Subtitle	5. Report Date
Test Results of Modified Electrical Charged Particle Generator for Application to Fog Dispersal	February 1983
	6. Performing Organization Code
7. Author(s)	8. Performing Organization Report No.
Walter Frost and Kao-Huah Huang	
	10. Work Unit No. M-405
9. Performing Organization Name and Address	11. Contract or Grant No.
FWG Associates, Inc. Rural Route #2, Box 271-A Tullahoma, Tennessee 37388	NAS8-34729
	13. Type of Report and Period Covered
12. Sponsoring Agency Name and Address	Contractor Report (Interim Report)
National Aeronautics and Space Administration Washington, D.C. 20546	14. Sponsoring Agency Code

15. Supplementary Notes

Prepared for Atmospheric Sciences Division, Space Science Laboratory, George C. Marshall Space Flight Center

Marshall Technical Monitor: Dennis W. Camp

16. Abstract

Modifications to a charged particle generator developed under NASA Contract NAS8-34729 for use in fog dispersal applications were made and additional testing carried out. The modified nozzle, however, did not work as planned, and reported results are for the unmodified nozzle. The addition of a positive displacement pump to supply the liquid water was highly successful.

Measurements of the generator output current were made with a cylindrical collector system as well as with the needle probe used in previous studies. Measurements with the cylindrical collector and the needle probe showed identical agreement within the variability of the experiment. A current of 20 μa or greater can be consistently produced with the modified system.

A high-voltage probe was purchased, and measurements of the corona voltage as well as the voltage variation in the charged particle jet were made. Electric fields in the vertical direction on the order of 10^6 v/m were measured. The voltage distribution along the centerline of the jet was compared with the numerical solutions of the Poisson equation and showed very good agreement.

Velocity measurements using a pitot tube were made. The resulting measurements were compared with theoretical and other reported experimental results. The measured data showed the appropriate trends and agreed well with reported results.

Based on the measured current-to-mass ratio from the charged particle generator, a calculation of the average droplet size was made. Droplet sizes were estimated to range between 0.8 and 0.4 μ. Using measured data, an analysis of the height to which the droplet can be dispersed by the charged particle generator was made. Although the mathematical model is highly simplified, the results indicated that particles would achieve heights on the order of 80 m.

It is anticipated that a new charged particle generator for operational and research applications will be developed based on the experience gained from testing of the prototype system.

17. Key Words (Suggested by Author(s))	18. Distribution Statement
Fog Fog Dispersal Visibility Charged Particle Fog Dispersal	Unclassified - Unlimited Subject Category 47

19. Security Classif. (of this report)	20. Security Classif. (of this page)	21. No. of Pages	22. Price
Unclassified	Unclassified	51	A04

For sale by National Technical Information Service, Springfield, Virginia 22161

NASA-Langley, 1983